TITLE: Merging empirical and mechanistic approaches to modeling aquatic visual foraging using a generalizable visual reaction distance model

AUTHORS: Sean K. Rohan[1,2,*], David A. Beauchamp[3], Timothy E. Essington[2], Adam G. Hansen[4]

AFFILIATIONS AND ADDRESSES:

[1]–National Marine Fisheries Service, Alaska Fisheries Science Center, National Oceanic and Atmospheric Administration, 7600 Sand Point Way NE, Seattle, WA 98115, USA.
[2]–University of Washington, School of Fishery and Aquatic Sciences, Box 355020, Seattle, WA 98195, USA.
[3]–U.S. Geological Survey, Western Fisheries Research Center, 6505 NE 65th Street, Seattle, WA, 98115, USA.
[4]–Colorado Parks and Wildlife, Aquatic Research Section, 317 W. Prospect Rd., Fort Collins, CO 80526, USA.

AUTHOR EMAILS ADDRESSES:

sean.rohan@noaa.gov
fadave@usgs.gov
essing@uw.edu
adam.hansen@state.co.us

CORRESPONDING AUTHOR:

[*]–sean.rohan@noaa.gov, tel: 206-526-4121

ABSTRACT

Visual encounter distance models are important tools for predicting how light and water clarity mediate visual predator-prey interactions that affect the structure and function of aquatic ecosystems at multiple spatial, temporal, and organizational scales. The two main varieties of visual encounter distance models, mechanistic and empirical, are used for similar purposes but take fundamentally different approaches to model development and have different strengths and weaknesses in terms of predictive accuracy, physical and biological interpretability of parameters, ability to incorporate outside information, and utility for knowledge transfer. To overcome weaknesses of existing mechanistic and empirical models and bridge the gap between approaches, we developed a generalized visual reaction distance model that relaxes assumptions of a widely-used mechanistic model that are violated in real predator-prey interactions. We compared the performance of the generalized visual reaction distance model to a widely used mechanistic model and an empirical visual encounter distance model by fitting models to data from four predator-prey experiments. The generalized visual reaction distance model substantially outperformed the other models in all cases based on fit to reaction distance data and presents an attractive alternative to prior models based on comparatively high predictive accuracy, use of interpretable parameters, and ability to incorporate outside information—characteristics that facilitate knowledge transfer.

KEYWORDS: behavioral ecology, visual foraging model, light and turbidity, predator-prey interactions, visual reaction distance

CONTENTS

1 INTRODUCTION

Visual encounter distance models are an important tool for understanding how visual predator-prey interactions affect the structure and function of aquatic ecosystems. Visual encounter distance models link conditions in the visual environment (light and water clarity) to the distance at which predator-prey interactions are initiated (Aksnes and Giske, 1993; Aksnes and Utne, 1997; Mazur and Beauchamp, 2003; Vogel and Beauchamp, 1999; Wright and O'Brien, 1984). The models provide a basis for answering questions about how visual predator-prey interactions affect ecosystems across multiple spatial, temporal, and organizational (e.g. population, community, whole ecosystem) scales (DeRobertis, 2002; Giske et al., 1994; Hansen and Beauchamp, 2015; Kitano et al., 2008; Maes et al., 2005).

We define three concepts that are important for understanding how visual predator-prey encounters are modeled in aquatic ecology: visual range, reaction distance, and encounter distance. Visual range is the distance at which an object (prey) is detectable to an animal (predator) based on visual sensory input exceeding the minimum threshold of detection for contrast, size, or motion of an animal's vision system. These thresholds are quantified using behavioral responses from conditioning experiments conducted with visual stimuli (e.g. Anthony, 1981), experiments that measure physiological (electrical) responses of the vision system response to stimuli of varying intensity (e.g. Horodysky et al., 2010; Naka and Rushton, 1966a; Semmelhack et al., 2014), histological and histological-physiological investigation of photoreceptor structure and function (e.g. Hairston, Jr. et al., 1982; Lythgoe, 1972; Warrant and Nilsson, 1998), and by fitting mechanistic models of visual range to data from predator-prey visual foraging experiments (e.g. Aksnes and Utne, 1997; Meager et al., 2010). Reaction distance

92 is the distance at which an animal exhibits a behavioral reaction towards a stimulus. In predator-
93 prey interactions, reaction distance is the result of both detection and co-evolved dynamics of
94 predator-prey interactions that determine whether a predator responds given detection of a
95 stimulus. Reaction distances are quantified using predator-prey experiments or in situ
96 observations of predator-prey interactions. We define encounter distance as the distance where a
97 predator initiates a predator-prey interaction within the context of a model. Encounter distance
98 can be synonymous with visual range or reaction distance, depending on how a visual encounter
99 distance model is constructed. Some approaches for calculating visual range based on minimum
100 detection criteria can combine information from physiological experiments, histological studies,
101 and behavioral conditioning studies, but do not account for behavior.
102 Visual encounter distance models are a key component of coupled visual foraging models
103 that predict prey encounter and consumption rates of predators as a function of light and water
104 clarity, prey distribution and density, and predator distribution. Two main varieties of visual
105 encounter distance models are used to characterize visual reactions of predators to prey,
106 mechanistic and empirical (i.e. phenomenological). Mechanistic and empirical models take
107 fundamentally different approaches to model development and parameterization. Mechanistic
108 models characterize visual range as a proxy for encounter distance based on individual physical
109 and biological components of predator-prey system. Mechanistic models are parameterized by
110 statistically fitting models to reaction distance data from visual foraging experiments (e.g.
111 Aksnes and Utne, 1997; Meager et al., 2010) or using morphological and functional traits of
112 predators and prey (Giske et al., 1994; Lovvorn et al., 2001; Nilsson et al., 2014; Ruxton and
113 Johnsen, 2016). Mechanistic models have a tendency to produce unrealistically large estimates of
114 reaction distance under conditions of low water clarity that are common in marine ecosystems.

As such, mechanistic models often impose generic and un-validated constraints on visual range, such as setting a minimum contrast threshold to avoid unrealistically low signal detection thresholds for photoreceptors (e.g. Ruxton and Johnsen, 2016) or setting maximum encounter distance equal to one predator body length (e.g. Fiksen et al., 2002; Langbehn and Varpe, 2017; Varpe and Fiksen, 2010). Empirical models are developed by fitting generic functional forms (e.g. polynomial, sigmoidal, piecewise polynomial) to reaction distance data from visual foraging experiments, with the best-fitting model used to predict visual encounter distances (Hansen et al., 2013; Holbrook et al., 2013; Keyler et al., 2019).

Mechanistic and empirical encounter distance models have different strengths and weaknesses, owing to different assumptions about how to represent processes that regulate visual predator-prey interactions. By using specific functional representations of physical and biological processes, mechanistic models assume that functional representations accurately represent the physical process by which image-forming light propagates through water, and the physiological-behavioral process of vision and reaction (Aksnes and Giske, 1993; Aksnes and Utne, 1997). The strength of mechanistic models is that they use physically interpretable parameters, which allows them to incorporate information beyond what may be available for a single experiment, predator or prey; this is useful because it is infeasible to conduct experiments with every predator-prey system (Lythgoe, 1972). However, a weakness is that if assumptions of mechanistic models are not met, they have limited ability to fit empirical data and may produce biased estimates of parameters and encounter distances.

In contrast to mechanistic models, empirical models make few assumptions about how physical or physiological-behavioral processes should be functionally represented. Consequently, empirical models may be more flexible and thereby provide a better fit to the data. A weakness is

that model terms do not always have a physical or biological interpretation outside the context of a specific predator-prey system, and parameters are not necessarily comparable among predators, prey, or experiments. The lack of a consistent structure and physically or biologically interpretable parameters makes it challenging—or even impossible—to apply empirical models to novel predator-prey systems or, in some cases, beyond the range of experimental treatments. This is an important limitation because it is not feasible to conduct experiments with every predator-prey system of interest.

Despite the different approaches to model development and parameterization, mechanistic and empirical visual encounter distance models are used to address similar questions. For example, a mechanistic model showed how reduced water clarity caused by eutrophication can allow tactile-feeding jellyfish to gain a competitive advantage over visually-feeding fish larvae, reducing the productivity of marine fish stocks (Eiane et al., 1999), while an empirical model demonstrated how reduced water clarity can reduce predation risk and increase foraging opportunity and productivity of lake-dwelling planktivorous fishes (Hansen and Beauchamp, 2015). Similarly, a mechanistic model suggested how the loss of Arctic sea-ice due to climate change may increase light and enhance the productivity of visually foraging pelagic fish stocks (Langbehn and Varpe, 2017), while an empirical model showed how increases in light due to anthropogenic light pollution can increase visual predation mortality for planktivorous fishes (Mazur and Beauchamp, 2006).

Ideally, visual encounter distance models should have physically and biologically interpretable parameters and apply consistent representations of the physical process of visual image transfer and the physiological-behavioral process of vision and reaction, but do so under a broader range of assumptions to improve model fits. In this way, a more standardized approach

161 can be used to estimate visual parameters from experimental data, thereby facilitating the transfer
162 and generalization of knowledge (Bouchet et al., 2019; Yates et al., 2018). Moreover, models
163 that use explicit structural representations of physiological-behavioral and physical processes
164 represent specific mechanistic hypotheses about how processes work. Thus, lack-of-fit can
165 provide insight into why a hypothesis failed and guide refinement or generation of new
166 hypotheses (Hilborn and Mangel, 1997).

167 It would be beneficial to develop a visual encounter distance model that mechanistically
168 characterizes physical and biological relationships in the visual encounter process, fits visual
169 reaction distance data well, can incorporate outside information, and facilitate knowledge
170 transfer. To that end, we developed a generalized visual reaction distance model that bridges the
171 gap between mechanistic and empirical modeling approaches by relaxing assumptions of the
172 widely-used Aksnes and Utne (1997) mechanistic model of visual range that appear to be
173 violated in real predator-prey interactions. The Aksnes and Utne (1997) model has seen
174 widespread use because it can be fitted to data from visual reaction distance experiments and
175 uses parameters that are physically and biologically interpretable. Because it uses physically and
176 biological interpretable parameters, the Aksnes and Utne model can be used to model predator-
177 prey systems where experimental data are not available (e.g. Aksnes and Giske, 1993; Langbehn
178 and Varpe, 2017; Lovvorn et al., 2001). Using data from four published experimental visual
179 foraging studies, we then compare the performance of the generalized visual reaction distance
180 model to the Aksnes and Utne model, and an empirical model that had the best fit among
181 multiple candidate empirical models in a visual reaction distance study (Hansen et al., 2013). We
182 chose these comparisons because they are representative of modeling options that are available
183 to experimentalists. We chose studies to provide a representative set of predator-prey systems

(planktivorous and piscivorous fish), sensory modes of foraging (visual and non-visual), environmental conditions (light and water clarity), and experimental configurations. Our primary aims were to evaluate whether assumptions of the Aksnes and Utne model were met, compare the performance of the generalized visual reaction distance model to empirical models, and examine how different modeling approaches affect parameter estimates and the precision and accuracy of predicted reaction distances. We show that the generalized visual reaction distance model fits reaction distance data better than the Aksnes and Utne model, but it retains physically and biologically interpretable parameters that are crucial for transferring information among predator-prey systems and allow the model to be used for predator-prey systems lacking experimental reaction distance data.

2 MATERIALS AND METHODS

We developed a generalized visual reaction distance model for aquatic predator-prey interactions by relaxing structural assumptions of the Aksnes and Utne model of visual range (Aksnes and Utne, 1997). By applying the model to a series of cases from the literature, we then compared the performance of various formulations of the generalized visual reaction distance model to the Aksnes and Utne model, and an empirical visual encounter distance model (Table 1). Parameters associated with these models are defined in Table 2.

2.1 Aksnes and Utne model of visual range

The Aksnes and Utne model combines mechanistic relationships from physics and physiology, the law of contrast reduction and Naka-Rushton function (Appendix A), to predict

visual range, as a proxy for visual encounter distance, based on the visual environment, functional light sensitivity of predator vision systems, and morphological traits of prey (Table 1; Table 2). In the Aksnes and Utne model, the condition for visual detection is

$$|C_0|\exp(-cr)\left(\frac{A_p}{r^2}\right)\left(\frac{E_{max}E_b}{K_e+E_b}\right) \geq \Delta S_e, \quad (1)$$

where $|C_0|$ is the inherent Weber contrast of a target (dimensionless), c is the beam attenuation coefficient of the medium (m^{-1}), r is viewing distance (m), A_p is the visible area of a target (m^2), E_{max} is the maximum irradiance processing level of an observer's vision system ($\mu E \cdot m^{-2} \cdot s^{-1}$), E_b is background irradiance in the environment ($\mu E \cdot m^{-2} \cdot s^{-1}$), K_e is the half-saturation level for processing of retinal irradiance ($\mu E \cdot m^{-2} \cdot s^{-1}$), and ΔS_e is the irradiance sensitivity threshold of the observer's vision system ($\mu E \cdot m^{-2} \cdot s^{-1}$). In the Aksnes and Utne model, a target (i.e. prey) is considered visible if the left side of Eqn. 1 is greater than or equal to ΔS_e. To solve for maximum visual range or reaction distance, ΔS_e can be combined into a composite saturation term, E' (dimensionless; $E' = E_{max} / \Delta S_e$,) which characterizes the visual capabilities of the observer, simplifying the model to

$$r^2\exp(cr) = |C_0|A_pE'\frac{E_b}{K_e+E_b}. \quad (2)$$

Inherent contrast, $|C_0|$, and prey area, A_p, are not measured in behavioral reaction distance experiments due to the complexities of prey orientation, predator viewing angle, color and brightness of prey, spectral sensitivity of the predator's vision system, and spectral characteristics of the light field. Thus, $|C_0|$, A_p and E' are generally estimated as composite predator-prey interaction term T (m^2), where $T = |C_0|A_pE'$.

When used to predict visual encounter distance between a predator and prey, the Aksnes and Utne model makes five key assumptions that, when violated, result in a lack-of-fit to

reaction distance data from visual foraging experiments: 1) predators detect prey visually; 2) predators view the object along a horizontal plane; 3) apparent contrast of an object decreases monotonically according to the law of contrast reduction; 4) reactions occur at the distance where apparent contrast of the object exceeds the minimum contrast threshold of the predator; and 5) the retinal-neural-behavioral response to changes in environmental light follows a Naka-Rushton function with $\alpha = 1$. There is evidence that real predator-prey interactions routinely violate the first four assumptions of the Aksnes and Utne model.

The first assumption of the Aksnes and Utne model can be violated because predators use senses other than vision to detect prey. When light levels fall below the minimum for visual detection of prey, reaction distances can approach an asymptote for some predator-prey systems (e.g. Hansen et al., 2013; Richmond et al., 2004). Filtering data a priori to ensure the model is only fit to visual reactions can prevent a violation of model assumptions, although the threshold light level between visual and non-visual reactions may not be obvious.

The second assumption that predators view prey along a horizontal plane is almost certainly violated in many real predator-prey interactions. In visual search, it is advantageous for predators to search for prey from below because downwelling light increases the luminance of the background, increasing the contrast of prey (e.g. Thetmeyer and Kils, 1995). To avoid issues of angular dependence and allow measurement of reaction distance at low light levels, some visual reaction distance experiments have constrained predator viewing angles by using shallow experimental arenas. Adding angular dependence to the Aksnes and Utne model would improve the flexibility of the model.

The third and fourth assumptions, regarding contrast reduction and contrast thresholds, can be violated in several ways, but reasons for a violation are inseparable based solely on

predator behavior. As turbidity increases from clear-water conditions, fishes exhibit an increase or no change in reaction distance to prey at low levels of turbidity, followed by a decrease at higher levels of turbidity (Hansen et al., 2013; Mazur and Beauchamp, 2003; Utne-Palm, 2002; Vogel and Beauchamp, 1999). Hypotheses to explain a lack-of-fit to turbidity are that suspendoids increase the visual contrast of prey against the background by affecting color and brightness contrast (physical effects hypothesis; Utne-Palm, 2002), that feeding motivation of predators increases at specific levels of turbidity due to acclimation (feeding motivation hypothesis; Boehlert and Morgan, 1985; Utne-Palm, 2002), or that reactions depend on a predator recognizing an object as prey based on apparent size, shape, and movement (ideal stimulus hypothesis; Hairston, Jr. et al., 1982; Semmelhack et al., 2014).

The third assumption may be violated because the law of contrast reduction may not apply to underwater visual foraging (Appendix A). The law of contrast reduction was originally derived for the atmosphere, where objects are visible at long distances (Lee et al., 2015). A key assumption used to analytically derive the law of contrast reduction for the atmosphere is that targets can be treated as point sources. This is likely violated in many underwater visibility applications because underwater objects become visible at distances that are orders-of-magnitude shorter distances than in air (Lee et al., 2015).

The fourth assumption, that reactions occur at the point where the apparent contrast of prey exceeds the minimum detectable contrast threshold, can be violated because detection precedes recognition and reaction, and detection and recognition of prey does not guarantee a reaction. An object becomes detectable (i.e. is within visual range) when image-forming light radiating from the object reaches an observer's photoreceptors and initiates a retinal-neural signaling response (phototransduction cascade) that exceeds some minimum threshold for

detection (Dowling, 2012). Signals are processed in the retina and brain, leading to recognition and reaction (Semmelhack et al., 2014). However, detection and recognition does not necessarily lead to reaction because reactions are mediated by the physiological state of a predator (e.g. hunger, stress), learning, and co-evolved dynamics of predator attack and prey defense, factors that may be considered extensions of the ideal stimulus and feeding motivation hypotheses.

Moreover, an object moving through the visual field of a predator presents an attentive cue that can play a role in detection, recognition, and reaction. Consequently, visual predators may react to mobile prey at greater distances than stationary prey (Utne-Palm, 1999), which is not explicitly represented in the Aksnes and Utne model.

2.2 Generalized visual reaction distance model (GVRDM)

We developed various formulations of a generalized visual reaction distance model to relax structural assumptions of the Aksnes and Utne model that appear violated in real predator-prey interactions (Table 1) and define the parameters associated with these models (Table 2). Starting from the Aksnes and Utne model (AUM.1), we added a non-visual reaction distance component to the model to relax the first assumption, as

$$\begin{matrix} {r_V}^2 \exp(r_V c) = |C_0| A_p E' \dfrac{E_b}{K_e + E_b} & if\ E_b \geq q \\ r_{NV} = D & if\ E_b < q \end{matrix}, \quad (3)$$

where D is non-visual reaction distance (m), and q is the light intensity threshold (μmol·photons·m^{-2}·s^{-1}) below which non-visual reaction distance exceeds visual reaction distance. Hereafter, we refer to this version of the Aksnes and Utne model with a non-visual reaction as AUM.2.

297 We relaxed the second assumption of the Aksnes and Utne model by incorporating
298 Duntley's angular contrast reduction equation (Duntley, 1952) into the model to allow non-
299 horizontal viewing angles, as

300 $$r_V{}^2 \exp\left(r_V(c - k_d \cos\theta)\right) = |C_0| A_p E' \frac{E_b}{K_e + E_b} \quad if\ E_b \geq q$$
$$r_{NV} = D \quad if\ E_b < q \tag{4}$$

301 where k_d is the downwelling diffuse attenuation coefficient (m^{-1}), and θ is the nadir viewing
302 angle (up = 0°, down = 180°).

303 To address the violation of the law of contrast reduction in underwater visibility
304 applications, we replaced the beam attenuation coefficient, c, with the effective attenuation
305 coefficient, κ (m^{-1}), based on the contrast reduction equation from Lee et al.'s (2015) underwater
306 visibility theory (Appendix A). However, for cases described below, we interchangeably used
307 the effective attenuation coefficient, κ, beam attenuation coefficient, c, and experimentally
308 measured absorption coefficients based on availability of experimental data although, the
309 coefficients characterize light transmission differently in terms of geometry.

310 Finally, we relaxed the third and fourth assumptions, that turbidity has a monotonic effect
311 on reaction distance and reactions occur at a specific contrast threshold, by including a dynamic
312 scaling function, $\omega(\cdot)$:

313 $$r_V{}^2 \exp\left(r_V(\kappa - k_d \cos\theta)\right) = \omega(\kappa)|C_0| A_p E' \frac{E_b}{K_e + E_b} \quad if\ E_b \geq q$$
$$r_{NV} = D \quad if\ E_b < q. \tag{5}$$

314 The dynamic scaling function models the effect of turbidity (e.g. effective attenuation
315 coefficient, κ) as a function of shape parameters β, δ, h:

316 $$\omega(\kappa) = \left(\beta + \frac{\delta^h \kappa^{h-1} \exp(-\delta\kappa)}{\Gamma(h)}\right). \tag{6}$$

317

318 The β parameter is dimensionless, but represents a turbidity-dependent change in contrast (i.e.
319 convergence to a new inherent contrast as turbidity increases). The h and δ parameters are
320 dimensionless and do not have a direct physical or biological interpretation outside of the context
321 of the dynamic scaling function. Rather, the parameters give the dynamic scaling function the
322 flexibility to take functional forms that represent hypotheses concerning the lack-of-fit of the
323 Aksnes and Utne model.

324 The model does not address specific violations of the fourth assumption. However, in
325 Case #3 (subsection 2.4.3) we examine how prey movement, a factor in the ideal stimulus
326 hypothesis, can be accounted for in the generalized visual reaction distance model.

327 The generalized visual reaction distance model does not provide a basis to test
328 mechanistic hypotheses about the lack-of-fit of the Aksnes and Utne model; rather it provides a
329 framework for testing whether structural assumptions of the Aksnes and Utne are violated in
330 visual foraging experiments. For plausible values of the effective attenuation coefficient, κ, the
331 Aksnes and Utne model is a special case of the generalized visual reaction distance model where
332 $\theta = 90°$, $q = 0$, $\beta = 1$, $h \to 0$, $\delta \to 0$, and $\varepsilon = 0$ or $b_f \to 0$.

333

334 2.3 Parameterization for model evaluation

335

336 We used the generalized visual reaction distance model, Aksnes and Utne model, and an
337 empirical broken-stick model for our cases (Tables 1–2; Appendix B). We reparameterized the
338 Aksnes and Utne model and generalized visual reaction distance model for our cases using the
339 composite predator-prey interaction term, T (m^2), to simplify the Aksnes and Utne model to

340 $$r^2 \exp(cr) = T \frac{E_b}{K_e + E_b}, \quad (7)$$

and the visual component of the generalized visual reaction distance model to

$$r_V{}^2 \exp\left(r_V(\kappa - k_d \cos\theta)\right) = \omega(\kappa) T \frac{E_b}{K_e + E_b} \quad if\ E_b \geq q. \tag{8}$$

2.4 Evaluation of models

We evaluated the performance of the generalized visual reaction distance model relative to the Aksnes and Utne model and an empirical encounter distance model. Specifically, we sought to evaluate whether assumptions of the Aksnes and Utne model were violated in real predator-prey interactions, whether the generalized visual reaction distance model performs as well as empirical models, and which version of the dynamic scaling function (with or without β) had the best performance in the generalized visual reaction distance model. We reviewed 32 visual foraging studies (65 predator-prey combinations among experiments) that involved manipulation of the visual environment and measurements of reaction distance (Table B2) and screened studies for inclusion in model evaluation based on suitability criteria (Table B1). Based on the screening criteria, we selected cases from four visual foraging studies for model evaluation based on our goal to include a representative set of predators (planktivores and piscivores), prey (fish and zooplankton; individuals and aggregations), and sensory modes of prey detection (visual and non-visual). Information about studies we reviewed and details of experimental designs from cases are described in Appendix B. Specific objectives and models used for each case are described below.

2.4.1 Case #1—Piscivore reacting to fish prey

We evaluated model performance for a piscivore system that may involve a non-visual reaction to prey at low light levels. We fit models to data from an experiment where yearling Chinook salmon *Oncorhynchus tshawytscha* reacted to juvenile rainbow trout *O. mykiss* under varying levels of light and turbidity (Hansen et al., 2013; Appendix B). In the experiments, Chinook salmon reaction distances approached an asymptote at ~50 cm at low light levels, potentially owing to a response to non-visual stimulus or an unexplained artifact of the experimental design. Because there was evidence of non-visual reaction, we used versions of the Aksnes and Utne model and generalized visual reaction distance model that included a non-visual reaction distance component (AUM.2, GVRDM.1, GVRDM.2; Table 1). We also fit a version of the best-fit empirical model (broken stick model [BSM]) from the original study to the data (Appendix C). Attack angles were not measured during the study so we assumed the nadir viewing angle was horizontal ($\theta = 90°$). Under this assumption, the diffuse attenuation coefficient, k_d, is irrelevant because $k_d \cos(90°)$ always equals zero.

2.4.2 Case #2—Planktivore reacting to group of ten zooplankton prey

We evaluated whether the dynamics governing detection of prey aggregations were the same as for detection of individual prey and estimated model parameters for Case #3. Thus, for Case #2, we fit models to data from an experiment where two-spotted goby *Gobius flavescens* reacted to aggregations of ten *Calanus finmarchicus*, a transparent calanoid copepod. Copepod aggregations were retained in 10 cm × 3 cm vials under varying levels of light and turbidity (Utne, 1997). No non-visual reactions were reported (i.e. no asymptote at low light levels) so we used formulations of the Aksnes and Utne model and generalized visual reaction distance model

without a non-visual reaction (AUM.1, GVRDM.3, GVRDM.4). Attack angles were not reported so we assumed $\theta = 90°$.

Because the Aksnes and Utne model uses beam attenuation, c, rather than effective attenuation coefficient, κ, we also evaluated whether this difference affected model performance (Aksnes and Utne, 1997; Appendix E: *Attenuation coefficients*).

2.4.3 Case #3—Planktivore reacting to single zooplankton

Case #3—We evaluated model performance for a planktivore reacting to individual prey, to assess if models could be used to simultaneously characterize the relative visibility of multiple prey types from the perspective of a predator and determine if the generalized visual reaction distance model and Aksnes and Utne model predicted similar visibility relationships among prey. We fit models to data from an experiment where two-spotted goby reacted to individual copepod (*C. finmarchicus/C. helgolandicus*) prey across a range of turbidities but only one light level, 20 $\mu E \cdot m^{-2} \cdot s^{-1}$ (Utne-Palm, 1999; Appendix B). Treatments used mobile transparent, immobile transparent, or mobile red-colored prey. No non-visual reactions were reported so we used models formulations without a non-visual reaction (AUM.1, GVRDM.3, GVRDM.4). Attack angles were not reported, so we assumed $\theta = 90°$. We included a different T parameter for each prey type (T_{TM} –transparent-mobile, T_{TI}–transparent immobile, T_{RM}–red-mobile). Because experimental light levels were constant, we could not estimate K_e using only Case #3 data. Instead, we parameterized models using the maximum likelihood estimates of K_e from Case #2.

2.4.4 Case #4—Planktivore reacting to single zooplankton, with angular dependence

We evaluated whether information about nadir viewing angle improved model fit to reaction distance data. To do so, we fit models to data from a planktivore experiment where stone moroko *Pseudorasbora parva* reacted to *Daphnia pulex* under varying levels of light and turbidity (Asaeda et al., 2002; Appendix B). The study was the only one we are aware of where both nadir viewing angles and reaction distances were reported. No non-visual reactions were reported so we used versions of the models without a non-visual component (AUM.1, GVRDM.3, and GVRDM.4; Table 1). To evaluate whether nadir viewing angle improved model fit, we compared models with nadir viewing angle to models where nadir viewing angle equaled 90° (Appendix E: *Angular dependence*).

2.5 Model fitting and comparison

For each case (subsections 2.4.1–2.4.4), variance in reaction distance increased as reaction distance increased, so we fit models assuming reaction distances had log-normally distributed error. We estimated separate variances for visual, σ_V, and non-visual, σ_{NV}, components of models because they involve different predator sensory processes that would presumably have different residual error structures. Additional details about model fitting are provided in Appendix B.

We used bias-corrected Akaike's Information Criterion (AIC_c) for model comparison and evaluated model fit and evidence for violations of assumptions based on visual inspection of Q-Q plots and residual plots.

3 RESULTS

3.1 Overall

The generalized visual reaction distance model substantially outperformed the Aksnes and Utne model in all cases, based on AIC_c (Table 3) and turbidity did not have a monotonic effect on reaction distance for any of the cases, which is shown by the dynamic scaling functions (Fig. 2). This suggests assumptions of the Aksnes and Utne model were violated in all of our cases. The Aksnes and Utne model had a lack-of-fit to turbidity, as shown by model fits across ranges of effective attenuation coefficient, κ (Figs. 3A, 4A, 5A), and patterns in model residuals in relation to κ (Figs. D1–D4), which also suggests assumptions of the Aksnes and Utne model were violated. The generalized visual reaction distance model had comparable or better fit than the Aksnes and Utne model across gradients of light (Figs. 3B, 4B).

Compared to the Aksnes and Utne model, the generalized visual reaction distance model tended to estimate that predators were less dark-adapted (higher K_e; Figs. 4D, 6C) and could process more light or had higher contrast sensitivity (higher T; Figs. 3D, 4D, 5C, 6C). The higher half-saturation level for retinal irradiance processing, K_e, predicted by the generalized visual reaction distance model for Cases #2–4 indicates that more light was necessary to stimulate a physiological-behavioral response to light. Higher values of the composite predator-prey interaction term, T, indicate a higher maximum retinal radiance processing capability, E_{max}, or lower threshold for the predator's vision system to detect changes in irradiance between the target and the background, ΔS_e. The latter is analogous to contrast sensitivity (Appendix A).

There was no evidence of turbidity-induced changes in prey contrast as versions of the generalized visual reaction distance model without a β parameter outperformed versions with a β parameter in all cases (Table 3). Additionally, for Cases #2–4, versions of the model with a β parameter had wider confidence intervals for parameters than models without β, indicating that inclusion of β inflated uncertainty in estimates of other parameters (Figs. 3D, 4D, 5C, 6C). Thus, we focused on versions of the model without β.

Across gradients of light and turbidity, reaction distances predicted by the generalized visual reaction distance model differed from the Aksnes and Utne model, as shown by fitted reaction distance surfaces for Cases #1–3 (Figs 3C, 4C, 5B). This is important because visual encounter distance models are often used to predict encounter distances well outside the range of experimental observations.

3.2 Cases

For Case #1, the generalized visual reaction distance model outperformed the broken-stick model based on AIC_c, indicating that it can perform at least as well as empirical models (Table 3). Despite the better fit of the generalized visual reaction distance model, predictions were generally similar between the generalized visual reaction distance model and broken stick model within the range of experimental conditions (Fig. 3A–B). However, beyond the range of experimental conditions there were considerable differences in predicted reaction distances between the models for Case #1 (Fig. 3C).

For Case #2, fitting models to adjusted beam attenuation, c, instead of the effective attenuation coefficient, κ, improved the fit of the Aksnes and Utne model and worsened the fit of the generalized visual reaction distance model (Table E1). Still, the generalized visual reaction

distance model outperformed the Aksnes and Utne model based on AIC_c. For the Aksnes and Utne model, K_e and T parameter estimates were ~2.1 and ~1.6 times higher than for the model with κ, respectively (Fig. E2). For the generalized visual reaction distance model, K_e did not change, but T was ~10.6 times higher than for models with κ (Fig. E2). Higher T indicates higher light processing capability or higher contrast sensitivity, while higher K_e indicate lower dark adaptation. Because light-intensity responses vary over orders-of-magnitude, small variations in K_e and T for the Aksnes and Utne model and K_e for the generalized visual reaction distance model would not substantially affect the predictive performance of models.

Processes regulating visual reactions of two-spotted goby to aggregations of ten copepods (Case #2) may have differed from those regulating reactions to individual copepods (Case #3). This is suggested by qualitative differences in the contour shapes between reaction distance surfaces for ten copepods (Fig. 4C) versus single copepods (Fig. 5B) and differences in dynamic scaling function parameters (Fig. 2, 4D, 5C). This difference may be an artifact of the experimental approach, the different levels at which data were aggregated for the cases, or because mechanisms that regulate visual reactions are functionally different between aggregations and individuals.

For Case #3, the generalized visual reaction distance model and Aksnes and Utne model both predicted that red mobile copepods (RM) were the most visible, followed by transparent mobile (TM), then transparent immobile (TI) copepods, as shown by fitted reaction distances (Fig. 5A–B) and the rank-order of T parameters for different prey ($T_{RM} > T_{TM} > T_{TI}$; Fig. 5C). The Aksnes and Utne model and generalized visual reaction distance model estimated nearly identical relative visibility relationships among prey, as T_{RM}:T_{TM}:T_{TI} was approximately 1.00:0.66:0.33 for both models. For the highest turbidity treatment (highest κ), predator reactions

to transparent immobile prey were based on a single observation, whereas all other observations were the mean of multiple reactions (Utne-Palm, 1999). This likely explains the single large outlier residual for transparent immobile prey for the generalized visual reaction distance model (Fig. D6).

In Case #4, the only case where viewing angles were observed, reaction distance was affected by nadir viewing angle, θ. The fit of the generalized visual reaction distance model was better using observed θ instead of $\theta = 90°$, as indicated by the lower AIC_c (Table F3). Viewing angle had a larger effect on reaction distance at higher turbidity (higher κ) when compared to low turbidity (Fig. 6A–B). The Aksnes and Utne model and generalized visual reaction distance model had similar trends in residual error across the range of θ, but the magnitude of residuals was much lower for the generalized visual reaction distance model (Fig. D7). Based on residuals of the generalized visual reaction distance model for $\theta > 100°$, the assumed angular relationship of the generalized visual reaction distance model may have been violated in Case #4 (Fig. D7). However, other factors may have affected the fit, such as: the experiment design, our digitization of plots with high point densities, our conversion of body lengths to meters, or our conversion of NTU to κ.

4 DISCUSSION

Overall, the generalized visual reaction distance model provides a balance between model fit and characterization of physical and biological relationships that is advantageous for modelling predator-prey interactions. The generalized visual reaction distance model fit better in all cases and is an attractive alternative to the Aksnes and Utne model and empirical models. The generalized visual reaction distance model is continuous and uses physically and biologically

interpretable parameters. This allows the model to accommodate new information and extend to novel circumstances. Unlike the Aksnes and Utne model, the generalized visual reaction distance model is not entirely based on measureable physical and biological properties because the dynamic scaling function does not represent a specific mechanism. Instead, the generalized visual reaction distance model provides a heuristic representation of multiple hypotheses (physical effects hypothesis, feeding motivation hypothesis, ideal stimulus hypothesis).

By using the dynamic scaling function, the generalized visual reaction distance model overcomes an important assumption of the Aksnes and Utne model: that visual range (and encounter distance) decreases monotonically with turbidity. This assumption is violated in real predator-prey interactions (see review by Utne-Palm [2002]), and may cause the Aksnes and Utne model to predict unreasonably high reaction distances at the low attenuation values that are common in marine ecosystems. As a solution, some studies have imposed a reaction distance constraint on the Aksnes and Utne model, such as setting the maximum reaction distance equal to one predator body length (e.g. Fiksen et al., 2002; Langbehn and Varpe, 2017; Varpe and Fiksen, 2010). Although the maximum reaction distance for some predator-prey interactions may approximately equal one predator body length (Richmond et al., 2004; Schwalbe and Webb, 2015; Utne, 1997), this cannot be considered a norm. Many predators react to prey at distances far-exceeding one predator body length (Asaeda et al., 2002; Blaxter, 1966; Hansen et al., 2013; Holbrook et al., 2013; Mazur and Beauchamp, 2003; Schmidt and O'Brien, 1982; Vinyard and O'Brien, 1976). In visual foraging models, constraining reaction distance to one body length may severely underestimate consumption rates because the models estimate consumption rates as a function of prey densities, handling time, and search volumes (i.e., volume searched per unit time), the latter of which is a function of reaction distance squared (search volume = swimming

546 speed×time elapsed×πr^2). The dynamic scaling function of the generalized visual reaction
547 distance model imposes an empirically-derived constraint on reaction distance, obviating the
548 need to impose arbitrary constraints. Further, if the generalized visual reaction distance model
549 can fit reaction distance data as well as empirical visual encounter distance models, it may
550 alleviate the need to use experimental designs that carefully stagger turbidity treatments to
551 identify critical thresholds for turbidity-dependent reaction distance, a primary design
552 consideration for some visual reaction distance experiments.

553 Comparing the relative visibility of multiple prey types in Case #3 illustrates an
554 advantage of using visual encounter distance models to characterize visibility. Traditionally,
555 differences in apparent size and contrast of prey have often been inferred from human
556 measurements of prey (e.g., contrast estimated from a photograph), and thus, may be prone to
557 measurement error and methodological biases. By contrast, we used the generalized visual
558 reaction distance model to estimate the relative visibility of multiple prey types, from the
559 perspective of a predator, using a single model that had a much better fit to the data than the
560 Aksnes and Utne model, but the same relative visibility relationship among prey as in the Aksnes
561 and Utne model. As such, the generalized visual reaction distance model can be used to validate
562 human-derived measures that characterize relative visibility (e.g., contrast estimated from a
563 photograph) and, due to the use of physically and biologically interpretable terms, improves our
564 knowledge transfer about the relative visibility of prey to other systems. This is important
565 because the core question for many visual foraging studies is how prey visibility (size and
566 contrast) interacts with the visual environment (light and water clarity) to affect predator-prey
567 linkages and ecosystem structure (e.g. Hansen and Beauchamp, 2014; Lovvorn et al., 2001;
568 Rosland and Giske, 1994).

569 The generalized visual reaction distance model can accommodate information about the
570 visual encounter process that is not explicitly included in the physical and biological terms. In
571 Case #3, for example, mobile and immobile transparent copepods would not have differences in
572 C_0 or A_p, so the difference between T_{MT} and T_{TI} is a movement effect that was not explicitly
573 represented in the model. The ratio T_{TM}/T_{TI} (1.5) can be interpreted as the proportional increase
574 in visibility due to movement (50%), although it is not clear how T_{TM} and T_{TI} are functionally
575 related because there is no generalizable relationship between motion and detection and we did
576 not have any information on movement speeds of mobile copepods from Case #3 experiments.
577 The model structure could be extended to accommodate known or hypothesized relationships.
578 For example, reaction distances can increase as a function of predator size (Mazur and
579 Beauchamp, 2003; Schmidt and O'Brien, 1982) due to ontogenetic changes in visual acuity,
580 spectral sensitivity, light sensitivity, or higher probability of capture success that increases the
581 profitability of longer distance attacks (Breck and Gitter, 1983; Britt et al., 2001; Hairston, Jr. et
582 al., 1982). Depending on what mechanism drives size-dependent variation in reaction distance,
583 the parameters K_e, ΔS_e, E', E_{max}, or T could be modeled as a function of predator size, as
584 suggested by Aksnes and Giske (1993).
585 In Case #1, the asymptotic reaction distance of adolescent Chinook salmon to juvenile
586 rainbow trout at low light levels may have resulted from a scale-dependent artifact of the
587 experimental design or a behaviorally-mediated change in visual prey detection, rather than a
588 result of different responses to visual and non-visual stimuli. Regardless, other studies have
589 shown that predators forage non-visually when light is limiting (e.g. Ryer et al., 2002), and that
590 non-visual reactions occur at distances greater than zero (Richmond et al., 2004). Unfortunately,
591 we were unable to fit the generalized visual reaction distance model to data from other studies

where non-visual reactions may have occurred because they did not have adequate sample sizes or include a sufficient range of variation in light levels.

Much of the data we used were not independent and we did not account for pseudoreplication in our primary analyses. Doing so would have underestimated the variability of individual reactions to prey (i.e. low σ_V, σ_{NV}, and σ). Further, the digitized data did not allow identification of unique predators or treatments for Cases #2–4. For Case #1, we could identify individual experimental trials in the original experimental data. To evaluate whether pseudoreplication affected our conclusions, we fit models to the mean reaction distances of trials for Case #1. Taking this approach, the generalized visual reaction distance model still outperformed the Aksnes and Utne model and empirical broken-stick model (Appendix E: *Pseudoreplication*).

Our approach to model fitting does not provide direct insight into the visual range of the predators because reaction distance is an indirect measure of visual range. Acknowledging the difference between visual range and reaction distance, Aksnes and Utne (1997) fit their model to data by first calculating the mean and standard deviation of reaction distance for each experimental light and turbidity treatment level, then fit their model to a visual range which they defined as the mean plus two standard deviations. While this approach may be reasonable, there is no inherent justification for such a definition of visual range. Multiple factors can drive variation in reaction distance, such as viewing angle, prey movement, prey orientation relative to the predator, spatial variation in the predator's visual acuity, feeding motivation of the predator, learning, social factors, and co-evolved attack-defense dynamics of a predator-prey system. Rather than accounting for differences between visual range and reaction distance *a priori*, we suggest a model with a well-behaved error structure could produce post hoc estimates of visual

615 range that are conceptually similar to the visual range definition of Aksnes and Utne (1997).
616 Such an approach would likely reduce the number of observations needed at each experimental
617 treatment level.

618 Although our statistical analyses of cases suggests that four assumptions of the Aksnes
619 and Utne model were violated, there was reasonable support for the fifth assumption, that the
620 light intensity-response for a predator reacting to prey is well-approximated by the Naka-Ruston
621 function (Appendix A). Other studies also support that the Naka-Ruston function affords a good
622 fit to experimental visual reaction distance data along a gradient of light, albeit using different
623 names, symbols, and quantities for functional representation. In the Appendix F: *Asymptotic*
624 *equivalence between empirical and mechanistic models*, we demonstrate that over short distances
625 and with low attenuation, empirical visual encounter distance models with Naka-Rushton
626 dynamics are asymptotically equivalent to the Aksnes and Utne model and generalized visual
627 reaction distance model.

628 Many studies we reviewed did not meet our screening criteria for cases because key
629 information were missing. One particularly common reason for exclusion was that turbidity was
630 reported in nephelometric turbidity units (NTUs) based on measurements from a nephelometric
631 turbidimeters (Table B2–B3), which cannot be readily converted to an optical property that
632 characterizes light transmission (e.g. beam attenuation, absorbance). Unlike beam
633 transmissometers and spectrophotometers that measure a reduction in light of known intensity
634 spectrum and intensity over a known distance, turbidimeters measure white (i.e. broad spectrum)
635 light scattered from a transmitted beam at a wide angle, typically centered at 90°, which does not
636 provide a direct measure of light transmission along a path (Davies-Colley and Smith, 2001;
637 Kirk, 2011). At best, NTUs are a relative measure of the volume scattering function at the angle

638 of the turbidimeter detector. NTUs tend to be closely correlated with beam attenuation for
639 highly-scattering suspended solids (e.g. kaolin, bentonite, diatomaceous earth) but not highly-
640 absorbing media (e.g. chlorophyll) (Kirk, 2011), and are therefore not particularly useful for
641 characterizing differences in light transmission for different media (e.g. kaolin versus
642 chlorophyll). We therefore encourage experimentalists to measure absorbance or beam
643 attenuation, use suspensions with known optical properties in known concentrations, or report
644 relationships between NTU and beam attenuation or absorbance in experiments. Although the
645 experiments spanned ranges generating the most dynamic visual responses (Appendix B), we
646 had limited ability to assess model performance across a broad environmental gradient because
647 simultaneous manipulation of light and turbidity only occurred in case #2. We suggest that future
648 visual reaction distance experiments be conducted across wider ranges of light and turbidity (i.e.,
649 employ greater environmental heterogeneity in experimental designs) to allow better assessment
650 of model performance. Acoustic technologies such as dual-frequency identification sonar
651 overcome limitations of video.

652 In real predator-prey interactions, there is stochastic variation in visual reaction distance
653 whereas the GVRDM predicts reaction distance as a threshold function of light, turbidity,
654 viewing angle, and traits of predators and prey. A possible way to extend the model to produce
655 more realistic characterizations of predator-prey interactions would be to modify the model to
656 predict the probability of reaction conditional on the distance between the predator and prey.
657 This potential extension could be examined using continuous particle tracking approaches in
658 experiments that allow continuous tracking of individual animals from video recordings. Such
659 approaches have shown promise for elucidating state-dependent probabilities of behavioural
660 transitions for interacting animals under experimental conditions (Bod'ová et al., 2018). A

similar approach may be useful for characterizing probabilities of a predator reacting to prey in visual foraging experiments.

5 CONCLUSIONS

Visual encounter distance models provide valuable insights into how visual processes affect the structure and function of aquatic ecosystems. The generalized visual reaction distance appears to be an attractive alternative to empirical models of reaction distance because it provides a good fit to reaction distance data from predator-prey systems within a single framework. It improves upon the Aksnes and Utne model by providing a better fit to empirical data when statistical analyses suggest assumptions of the Aksnes and Utne model are violated, although it does not provide a means to test hypotheses concerning why assumptions may be violated. We speculate that testing these hypotheses will require improvements to the model based on a deeper integration of dynamics involved in predator-prey interactions that arise from physics, physiology, and ethology.

6 ACKNOWLEDGMENTS

We are grateful to Lyle Britt, Ellis Loew, Jeff Napp, Jennifer Schulien, and Andy Whitehouse for constructive comments on an earlier version of this manuscript. We greatly appreciate comments from two anonymous reviewers and the associate editor, whose helpful suggestions greatly improved this manuscript. We thank Anne-Christine Utne-Palm for providing

clarification about experimental methods. Any use of trade, firm, or product names is for descriptive purposes only and does not imply endorsement by the U.S. Government.

7 FUNDING SOURCES

NOAA Fisheries and the Environment Program (FATE)

8 DATA STATEMENT

Upon acceptance, digitized data for cases #2–4 will be made publically available through an online GitHub repository (Sean-Rohan-NOAA/GVRDM) and a gold standard back-up will be retained by the NOAA Alaska Fisheries Science Center. Requests for digitized data for case #1 can be submitted to A.G. Hansen.

9 REFERENCES

Aksnes, D.L., Giske, J., 1993. A theoretical model of aquatic visual feeding. Ecol. Modell. 67, 233–250. https://doi.org/10.1016/0304-3800(93)90007-F

Aksnes, D.L., Utne, A.C.W., 1997. A revised model of visual range in fish. Sarsia 82, 137–147. https://doi.org/10.1080/00364827.1997.10413647

Anthony, P.D., 1981. Visual contrast thresholds in the cod *Gadus morhua* L. J. Fish Biol. 19, 87–103. https://doi.org/10.1111/j.1095-8649.1981.tb05814.x

Asaeda, T., Park, B.K., Manatunge, J., 2002. Characteristics of reaction field and the reactive

distance of a planktivore, *Pseudorasbora parva* (Cyprinidae), in various environmental conditions. Hydrobiologia 489, 29–43. https://doi.org/10.1023/A:1023298823106

Blaxter, J.H.S., 1966. The effect of light intensity on the feeding ecology of herring, in: Bainbridge, R., Evans, G.C., Rackham, O. (Eds.), Light as an Ecological Factor: A Symposium of the British Ecological Society Cambridge 30th March-1 April 1965. John Wiley & Sons Inc, New York, pp. 393–409.

Bod'ová, K., Mitchell, G.J., Harpaz, R., Schneidman, E., Tkačik, G., 2018. Probabilistic models of individual and collective animal behavior. PLoS One 13, e0193049. https://doi.org/10.1371/journal.pone.0193049

Boehlert, G.W., Morgan, J.B., 1985. Turbidity enhances feeding abilities of larval Pacific herring, *Clupea harengus pallasi*. Hydrobiologia 123, 161–170.

Bouchet, P.J., Peterson, A.T., Zurell, D., Dormann, C.F., Schoeman, D., Ross, R.E., Snelgrove, P., Sequeira, A.M.M., Whittingham, M.J., Wang, L., Rapacciuolo, G., Oppel, S., Mellin, C., Lauria, V., Krishnakumar, P.K., Jones, A.R., Heinänen, S., Heikkinen, R.K., Gregr, E.J., Fielding, A.H., Caley, M.J., Barbosa, A.M., Bamford, A.J., Lozano-Montes, H., Parnell, S., Wenger, S., Yates, K.L., 2019. Better model transfers require knowledge of mechanisms. Trends Ecol. Evol. 34, 489–490. https://doi.org/10.1016/j.tree.2019.04.006

Breck, J.E., Gitter, M.J., 1983. Effect of fish size on the reactive distance of bluegill (*Lepomis macrochirus*) sunfish. Can. J. Fish. Aquat. Sci. 40, 162–167. https://doi.org/10.1139/f83-026

Britt, L.L., Loew, E.R., McFarland, W.N., 2001. Visual pigments in the early life stages of Pacific northwest marine fishes. J. Exp. Biol. 204, 2581–2587.

Davies-Colley, R.J., Smith, D.G., 2001. Turbidity, suspended sediment, and water clarity: A

review. J. Am. Water Resour. Assoc. 37, 1085–1101. https://doi.org/10.1111/j.1752-1688.2001.tb03624.x

DeRobertis, A., 2002. Size-dependent visual predation risk and the timing of vertical migration: An optimization model. Limnol. Oceanogr. 47, 925–933.

Dowling, J.E., 2012. The retina: an approachable part of the brain, Revised Ed. ed. The Belknap Press of Harvard University Press, Cambridge, MA.

Duntley, S.Q., 1952. The visibility of submerged objects. Cambridge, Massachusetts.

Eiane, K., Aksnes, D.L., Bagøien, E., Kaartvedt, S., 1999. Fish or jellies — a question of visibility? Limnol. Oceanogr. 44, 1352–1357. https://doi.org/10.4319/lo.1999.44.5.1352

Fiksen, Ø., Aksnes, D.L., Flyum, M.H., Giske, J., 2002. The influence of turbidity on growth and survival of fish larvae: a numerical analysis. Hydrobiologia 484, 49–59. https://doi.org/10.1023/A:1021396719733

Giske, J., Aksnes, D.L., Fiksen, Ø., 1994. Visual predators, environmental variables and zooplankton mortality risk. Vie Milieu 44, 1–9.

Hairston, Jr., N.G., Li, K.T., Easter, Jr., S.S., 1982. Fish vision and the detection of planktonic prey. Science (80-.). 218, 1240–1242.

Hansen, A.G., Beauchamp, D.A., 2015. Latitudinal and photic effects on diel foraging and predation risk in freshwater pelagic ecosystems. J. Anim. Ecol. 84, 532–544. https://doi.org/10.1111/1365-2656.12295

Hansen, A.G., Beauchamp, D.A., 2014. Effects of prey abundance, distribution, visual contrast and morphology on selection by a pelagic piscivore. Freshw. Biol. 59, 2328–2341. https://doi.org/10.1111/fwb.12436

Hansen, A.G., Beauchamp, D.A., Schoen, E.R., 2013. Visual prey detection responses of

751 piscivorous trout and salmon: Effects of light, turbidity, and prey size. Trans. Am. Fish.
752 Soc. 142, 854–867. https://doi.org/10.1080/00028487.2013.785978
753 Hilborn, R., Mangel, M., 1997. The ecological detective: Confronting models with data.
754 Princeton University Press.
755 Holbrook, B. V., Hrabik, T.R., Branstrator, D.K., Mensinger, A.F., 2013. Foraging mechanisms
756 of age-0 lake trout (*Salvelinus namaycush*). J. Great Lakes Res. 39, 128–137.
757 https://doi.org/10.1016/j.jglr.2012.12.008
758 Horodysky, A.Z., Brill, R.W., Warrant, E.J., Musick, J.A., Latour, R.J., 2010. Comparative
759 visual function in four piscivorous fishes inhabiting Chesapeake Bay. J. Exp. Biol. 213,
760 1751–1761. https://doi.org/10.1242/jeb.038117
761 Keyler, T.D., Hrabik, T.R., Mensinger, A.F., Rogers, L.S., Gorman, O.T., 2019. Effect of light
762 intensity and substrate type on siscowet lake trout (*Salvelinus namaycush siscowet*)
763 predation on deepwater sculpin (Myoxocephalus thompsonii). Hydrobiologia 840, 77–88.
764 https://doi.org/10.1007/s10750-019-3944-5
765 Kirk, J.T.O., 2011. Light and photosynthesis in aquatic ecosystems, 3rd ed. Cambridge
766 University Press, New York.
767 Kitano, J., Bolnick, D.I., Beauchamp, D.A., Mazur, M.M., Mori, S., Nakano, S., Peichel, C.L.,
768 2008. Reverse evolution of armour plates in the threespine stickleback. Curr. Biol. 18, 744–
769 769.
770 Langbehn, T.J., Varpe, Ø., 2017. Sea-ice loss boosts visual search: Fish foraging and changing
771 pelagic interactions in polar oceans. Glob. Chang. Biol. 23, 5318–5330.
772 https://doi.org/10.1111/gcb.13797
773 Lee, Z., Shang, S., Hu, C., Du, K., Weidemann, A., Hou, W., Lin, J., Lin, G., 2015. Secchi disk

774 depth: A new theory and mechanistic model for underwater visibility. Remote Sens.
775 Environ. 169, 139–149. https://doi.org/10.1016/j.rse.2015.08.002
776 Lovvorn, J.R., Baduini, C.L., Hunt Jr., G.L., 2001. Modeling underwater visual and filter feeding
777 by planktivorous shearwaters in unusual sea conditions. Ecology 82, 2342–2356.
778 Lythgoe, J.., 1972. The adaptation of visual pigments to the photic environment, in: Dartnell,
779 H.J.A. (Ed.), The Handbook of Sensory Physiology VII/1. Springer, pp. 566–603.
780 Maes, J., Limburg, K.E., van de Putte, A., Ollevier, F., 2005. A spatially explicit, individual-
781 based model to assess the role of estuarine nurseries in the early life history of North Sea
782 herring, *Clupea harengus*. Fish. Oceanogr. 14, 17–31. https://doi.org/10.1111/j.1365-
783 2419.2004.00300.x
784 Mazur, M.M., Beauchamp, D.A., 2006. Linking piscivory to spatial-temporal distributions of
785 pelagic prey fishes with a visual foraging model. J. Fish Biol. 69, 151–175.
786 https://doi.org/10.1111/j.1095-8649.2006.01075.x
787 Mazur, M.M., Beauchamp, D.A., 2003. A comparison of visual prey detection among species of
788 piscivorous salmonids: Effects of light and low turbidities. Environ. Biol. Fishes 67, 397–
789 405. https://doi.org/10.1023/A:1025807711512
790 Meager, J.J., Moberg, O., Strand, E., Utne-Palm, A., 2010. Effects of light intensity on visual
791 prey detection by juvenile Atlantic cod (*Gadus morhua* L.). Mar. Freshw. Behav. Physiol.
792 43, 99–108. https://doi.org/http://dx.doi.org/10.1080/10236241003798910
793 Naka, K.I., Rushton, W.A.H., 1966. S-potentials from colour units in the retina of fish
794 (Cyprinidae). J. Physiol. 185, 536–555.
795 Nilsson, D.E., Warrant, E., Johnsen, S., 2014. Computational visual ecology in the pelagic realm.
796 Philos. Trans. R. Soc. B Biol. Sci. 369. https://doi.org/10.1098/rstb.2013.0038

797 Richmond, H.E., Hrabik, T.R., Mensinger, A.F., 2004. Light intensity, prey detection and
798 foraging mechanisms of age 0 year yellow perch. J. Fish Biol. 65, 195–205.
799 https://doi.org/10.1111/j.0022-1112.2004.00444.x
800 Rosland, R., Giske, J., 1994. A Dynamic Optimization Model of the Diel Vertical-Distribution of
801 a Pelagic Planktivorous Fish. Prog. Oceanogr. 34, 1–43. https://doi.org/10.1016/0079-
802 6611(94)90025-6
803 Ruxton, G.D., Johnsen, S., 2016. The effect of aggregation on visibility in open water. Proc. R.
804 Soc. B Biol. Sci. 283.
805 Ryer, C.H., Lawton, A., Lopez, R.J., Olla, B.L., 2002. A comparison of the functional ecology of
806 visual vs. nonvisual foraging in two planktivorous marine fishes. Can. J. Fish. Aquat. Sci.
807 59, 1305–1314. https://doi.org/10.1139/f02-097
808 Schmidt, D., O'Brien, W.J., 1982. Planktivorous feeding ecology of Arctic grayling (*Thymallus*
809 *arcticus*). Can. J. Fish. Aquat. Sci. 39, 475–482. https://doi.org/10.1155/2011/352451
810 Schwalbe, M.A.B., Webb, J.F., 2015. The effect of light intensity on prey detection behavior in
811 two Lake Malawi cichlids, *Aulonocara stuartgranti* and *Tramitichromis* sp. J. Comp.
812 Physiol. A Neuroethol. Sensory, Neural, Behav. Physiol. 201, 341–356.
813 https://doi.org/10.1007/s00359-015-0982-y
814 Semmelhack, J.L., Donovan, J.C., Thiele, T.R., Kuehn, E., Francisco, S., Francisco, S., 2014. A
815 dedicated visual pathway for prey detection in larval zebrafish. Elife 3, 1–19.
816 https://doi.org/10.7554/eLife.04878
817 Thetmeyer, H., Kils, U., 1995. To see and not be seen: the visibility of predator and prey with
818 respect to feeding behaviour. Mar. Ecol. Prog. Ser. 126, 1–8.
819 https://doi.org/10.3354/meps126001

820 Utne-Palm, A., 2002. Visual feeding of fish in a turbid environment: Physical and behavioural
821 aspects. Mar. Freshw. Behav. Physiol. 35, 111–128.
822 https://doi.org/10.1080/10236240290025644
823 Utne-Palm, A., 1999. The effect of prey mobility, prey contrast, turbidity and spectral
824 composition on the reaction distance of *Gobiusculus flavescens* to its planktonic prey. J.
825 Fish Biol. 54, 1244–1258. https://doi.org/10.1111/j.1095-8649.1999.tb02052.x
826 Utne, A., 1997. The effect of turbidity and illumination on the reaction distance and search time
827 of the marine planktivore *Gobiusculus flavescens*. J. Fish Biol. 50, 926–938.
828 https://doi.org/10.1111/j.1095-8649.1997.tb01619.x
829 Varpe, Ø., Fiksen, Ø., 2010. Seasonal plankton-fish interactions: light regime, prey phenology,
830 and herring foraging. Ecology 91, 311–318.
831 Vinyard, G.L., O'Brien, W.J., 1976. Effects of light and turbidity on the reactive distance of
832 bluegill (*Lepomis macrochirus*). J. Fish. Res. Board Canada 33, 2845–2849.
833 Vogel, J.L., Beauchamp, D.A., 1999. Effects of light, prey size, and turbidity on reaction
834 distances of lake trout (*Salvelinus namaycush*) to salmonid prey. Can. J. Fish. Aquat. Sci.
835 56, 1293–1297. https://doi.org/10.1139/cjfas-56-7-1293
836 Warrant, E.J., Nilsson, D., 1998. Absorption of White Light in Photoreceptors. Vision Res. 38,
837 195–207. https://doi.org/10.1016/S0042-6989(97)00151-X
838 Wright, D.I., O'Brien, W.J., 1984. The development and field test of a tactical model of the
839 planktivorous feeding of white crappie (*Pomoxis annularis*). Ecol. Monogr. 54, 65–98.
840 Yates, K.L., Bouchet, P.J., Caley, M.J., Mengersen, K., Randin, C.F., Parnell, S., Fielding, A.H.,
841 Bamford, A.J., Ban, S., Barbosa, A.M., Dormann, C.F., Elith, J., Embling, C.B., Ervin,
842 G.N., Fisher, R., Gould, S., Graf, R.F., Gregr, E.J., Halpin, P.N., Heikkinen, R.K.,

Heinänen, S., Jones, A.R., Krishnakumar, P.K., Lauria, V., Lozano-Montes, H., Mannocci, L., Mellin, C., Mesgaran, M.B., Moreno-Amat, E., Mormede, S., Novaczek, E., Oppel, S., Ortuño Crespo, G., Peterson, A.T., Rapacciuolo, G., Roberts, J.J., Ross, R.E., Scales, K.L., Schoeman, D., Snelgrove, P., Sundblad, G., Thuiller, W., Torres, L.G., Verbruggen, H., Wang, L., Wenger, S., Whittingham, M.J., Zharikov, Y., Zurell, D., Sequeira, A.M.M., 2018. Outstanding challenges in the transferability of ecological models. Trends Ecol. Evol. 33, 790–802. https://doi.org/10.1016/j.tree.2018.08.001

TABLES

853 Table 1. Models used for case studies.

Abbrev.	Description	Model
AUM.1	Aksnes and Utne model	$r_V^2 \exp(cr_V) = T\frac{E_b}{K_e+E_b}$
AUM.2	Aksnes and Utne model with non-visual reaction	$r_V{}^2 \exp(cr_V) = T\frac{E_b}{K_e+E_b} \quad if\ E_b \geq q$ $r_{NV} = D \quad if\ E_b < q$
GVRDM.1	Generalized visual reaction distance model with non-visual reaction and β	$r_V{}^2 \exp(r_V(-k_d \cos\theta)) = \omega(\kappa)T_i\frac{E_b}{K_e+E_b} \quad if\ E_b \geq q$ $r_{NV} = D \quad if\ E_b < q$ $\omega(\kappa) = \beta + \frac{\delta^h \kappa^{h-1}\exp(-\delta\kappa)}{\Gamma(h)}$
GVRDM.2	Generalized visual reaction distance model with non-visual reaction, without β	$r_V{}^2 \exp(r_V(\kappa - k_d \cos\theta)) = \omega(\kappa)T\frac{E_b}{K_e+E_b} \quad if\ E_b \geq q$ $r_{NV} = D \quad if\ E_b < q$ $\omega(\kappa) = \frac{\delta^h \kappa^{h-1}\exp(-\delta\kappa)}{\Gamma(h)}$
GVRDM.3	Generalized visual reaction distance model and without non-visual reaction, with β	$r_V{}^2 \exp(r_V(\kappa - k_d \cos\theta)) = \omega(\kappa)T_i\frac{E_b}{K_e+E_b}$ $\omega(\kappa) = \beta + \frac{\delta^h \kappa^{h-1}\exp(-\delta\kappa)}{\Gamma(h)}$
GVRDM.4	Generalized visual reaction distance model without non-visual reaction or β	$r_V{}^2 \exp(r_V(\kappa - k_d \cos\theta)) = \omega(\kappa)T\frac{E_b}{K_e+E_b}$ $\omega(\kappa) = \frac{\delta^h \kappa^{h-1}\exp(-\delta\kappa)}{\Gamma(h)}$
BSM	Broken-stick model	$r = \begin{cases}(v + wE_b)p & if\ E_b > q_E \\ r_{max}p & if\ E_b \leq q_E\end{cases}$ $p = \begin{cases}1 & if\ c \leq q_\kappa \\ e^{y(\kappa - q_\kappa)} & if\ c > q_\kappa\end{cases}$

854

855 Table 1. Model terms and descriptions.

Term	Units	Description
Aksnes and Utne model and generalized visual reaction distance model		
A_p	m^2	Visible area of prey
β	dimensionless	Dynamic scaling function intercept parameter
b_f	m^{-1}	Forward scattering coefficient (Appendix A)
c	m^{-1}	Beam attenuation coefficient
C_0	dimensionless	Inherent Weber contrast of prey
δ	dimensionless	Dynamic scaling function rate parameter
D	m	Non-visual reaction distance
E_b	$\mu E \cdot m^{-2} \cdot s^{-1}$	Background irradiance
E_{max}	$\mu E \cdot m^{-2} \cdot s^{-1}$	Maximum irradiance processing capability of the retina
E'	dimensionless	Composite saturation parameter ($E' = E_{max}\Delta S_e^{-1}$)
ε	dimensionless	Scaling factor for b_f (Appendix A)
h	dimensionless	Dynamic scaling function shape parameter
κ	m^{-1}	Effective attenuation coefficient $\kappa = c - \varepsilon b_f$ (Appendix A)
k_d	m^{-1}	Downwelling diffuse attenuation coefficient
K_e	$\mu E \cdot m^{-2} \cdot s^{-1}$	Half-saturation for irradiance processing
q	$\mu E \cdot m^{-2} \cdot s^{-1}$	Visual reaction threshold
r	m	Reaction distance
r_{NV}	m	Non-visual reaction distance
r_V	m	Visual reaction distance
σ_{NV}		Standard deviation of non-visual reaction distance
σ_V		Standard deviation of visual reaction distance
ΔS_e	$\mu E \cdot m^{-2} \cdot s^{-1}$	Sensitivity threshold of the vision system for detecting changes in irradiance
T	m^2	Composite predator-prey interaction term ($T = \lvert C_0 \rvert A_p E'$)
T_i	m^2	Composite predator-prey interaction term for prey type i (used in Case #3)
θ	°	Nadir viewing angle (up = 0°, down = 180°)
Broken-stick model		
c	m^{-1}	Beam attenuation coefficient
E_b	$\mu E \cdot m^{-2} \cdot s^{-1}$	Background irradiance
κ	m^{-1}	Effective attenuation coefficient $\kappa = c - \varepsilon b_f$
p	dimensionless	Turbidity scaling parameter
q_κ	m^{-1}	Minimum turbidity threshold for κ
q_E	$\mu E \cdot m^{-2} \cdot s^{-1}$	Saturation intensity threshold for E_b
r_{max}	m	Maximum reaction distance
σ		Standard deviation of reaction distance
v	m	Light function intercept
w	$m^3 \cdot s \cdot \mu E^{-1}$	Light function slope
y	m	Turbidity function slope

856

857 Table 2. Summary of model fits showing the model, number of parameters, sample size (n), and
858 AICc differences between the model and best model (ΔAICc). For each case, the model with the
859 lowest AICc is shown in bold.

Model	Par. (#)	n	ΔAIC_c
Case #1 – Chinook salmon (predator), rainbow trout (prey)			
AUM.2	6	629	155.0
GVRDM.1	9	629	1.6
GVRDM.2	**8**	**629**	**0.0**
BSM	7	629	17.1
Case #2 – Two-spotted goby (predator), group of ten *Calanus* (prey)			
AUM.1	3	214	64.1
GVRDM.3	6	214	1.4
GVRDM.4	**5**	**214**	**0.0**
Case #3 – Two-spotted goby (predator), single *Calanus* (prey)			
AUM.1	6	24	32.1
GVRDM.3	9	24	2.9
GVRDM.4	**8**	**24**	**0.0**
Case #4 – Stone moroko (predator), *Daphnia pulex* (prey)			
AUM.1	3	177	233.4
GVRDM.3	6	177	1.0
GVRDM.4	**5**	**177**	**0.0**

860

861 FIGURES

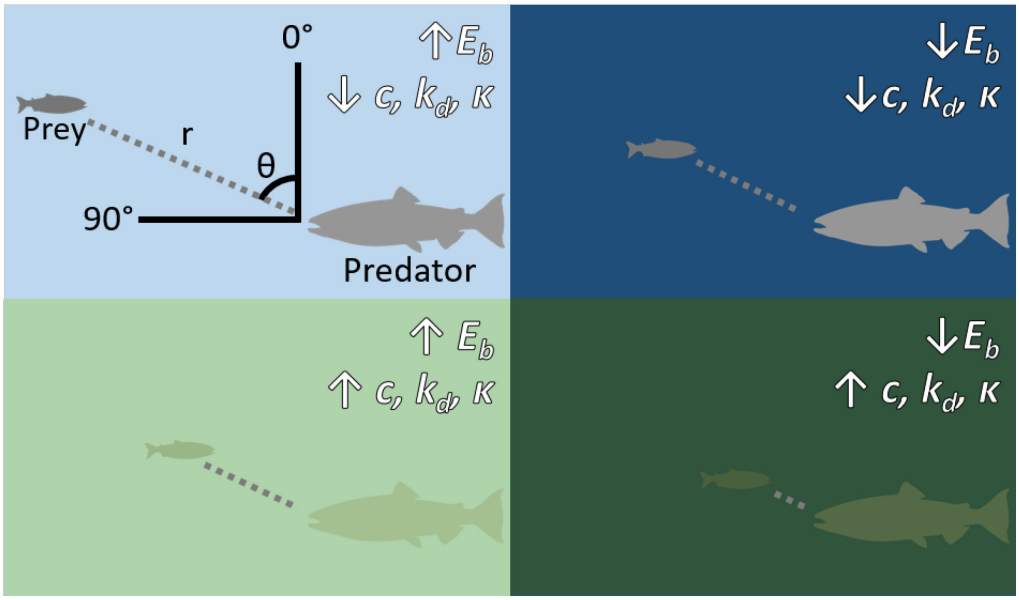

862

863 Figure 1. Conceptual diagram of the reaction distance of a predator to prey under conditions of light (i.e.,
864 background irradiance, E_b) and water clarity (beam attenuation (c), diffuse downwelling attenuation coefficient (k_d),
865 and effective attenuation coefficient (κ)), where r = reaction distance and θ = nadir viewing angle. Clockwise from
866 the top left: high light/high water clarity, low light/high water clarity, high light/low water clarity, low light/low
867 water clarity.

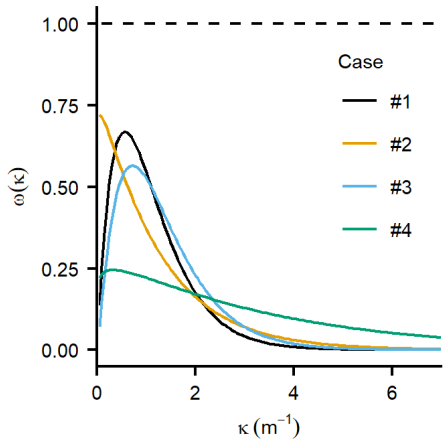

868

869 Figure 2. Dynamic scaling function, ω(κ), for the best-fit version of the generalized visual reaction distance model
870 for each Case. None of the dynamic scaling functions include an intercept term for the dynamic scaling function (β
871 parameter). Horizontal dashed line denotes asymptotic expectation under the Aksnes and Utne model.

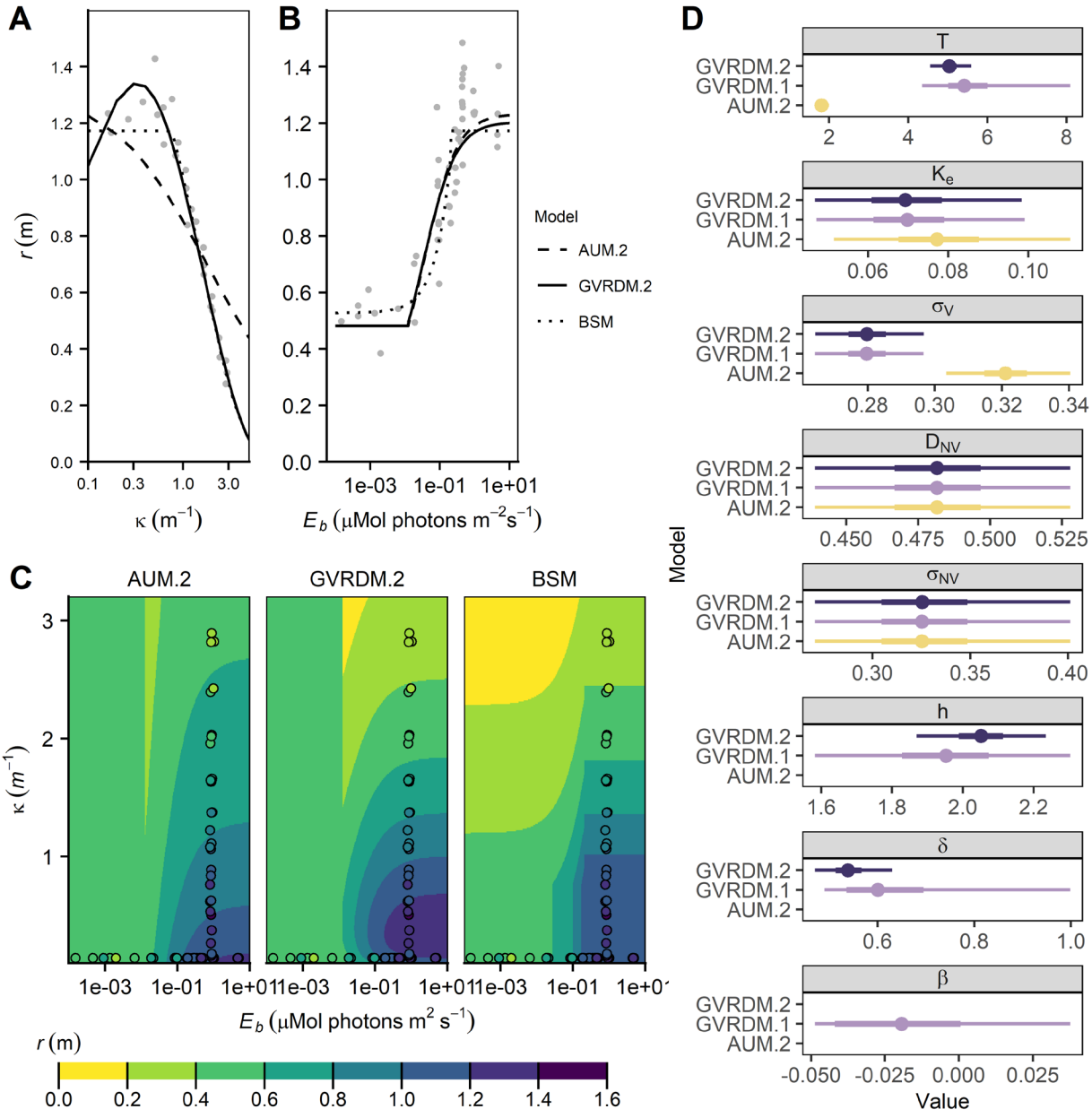
A
B
C
D
r (m)
κ (m⁻¹)
Eb (µMol photons m⁻²s⁻¹)
Model
AUM.2
GVRDM.2
BSM
Eb (µMol photons m² s⁻¹)
r (m)
T
Ke
σV
DNV
σNV
h
δ
β
GVRDM.2
GVRDM.1
AUM.2
Value

872

Figure 3. Case #1—Reaction distances and parameter estimates for yearling Chinook salmon reacting to juvenile rainbow trout along gradients of effective attenuation coefficient, κ, and light, $E_{b,}$ for the Aksnes and Utne model with a non-visual reaction (AUM.2), generalized visual reaction distance model with a non-visual reaction, without β (GVRDM.2), and empirical broken stick model (BSM). Panels show (A) fitted (lines) and observed (points) reaction distance along a gradient of κ under constant $E_b \approx 0.75$ μMol photons $m^{-2}s^{-1}$, where points denote means for individual experimental trials; (B) fitted (lines) and observed (point) reaction distances along a gradient of E_b under constant $\kappa = 0.1408$; (C) fitted reaction distance surfaces and mean reaction distances for individual experimental trials (points) where fill color shows reaction distance; (D) parameter estimates for AUM.2, GVRDM.1, and GVRDM.2 where points denote the mean and thick and thin lines denote the 50% and 95% confidence intervals, respectively.

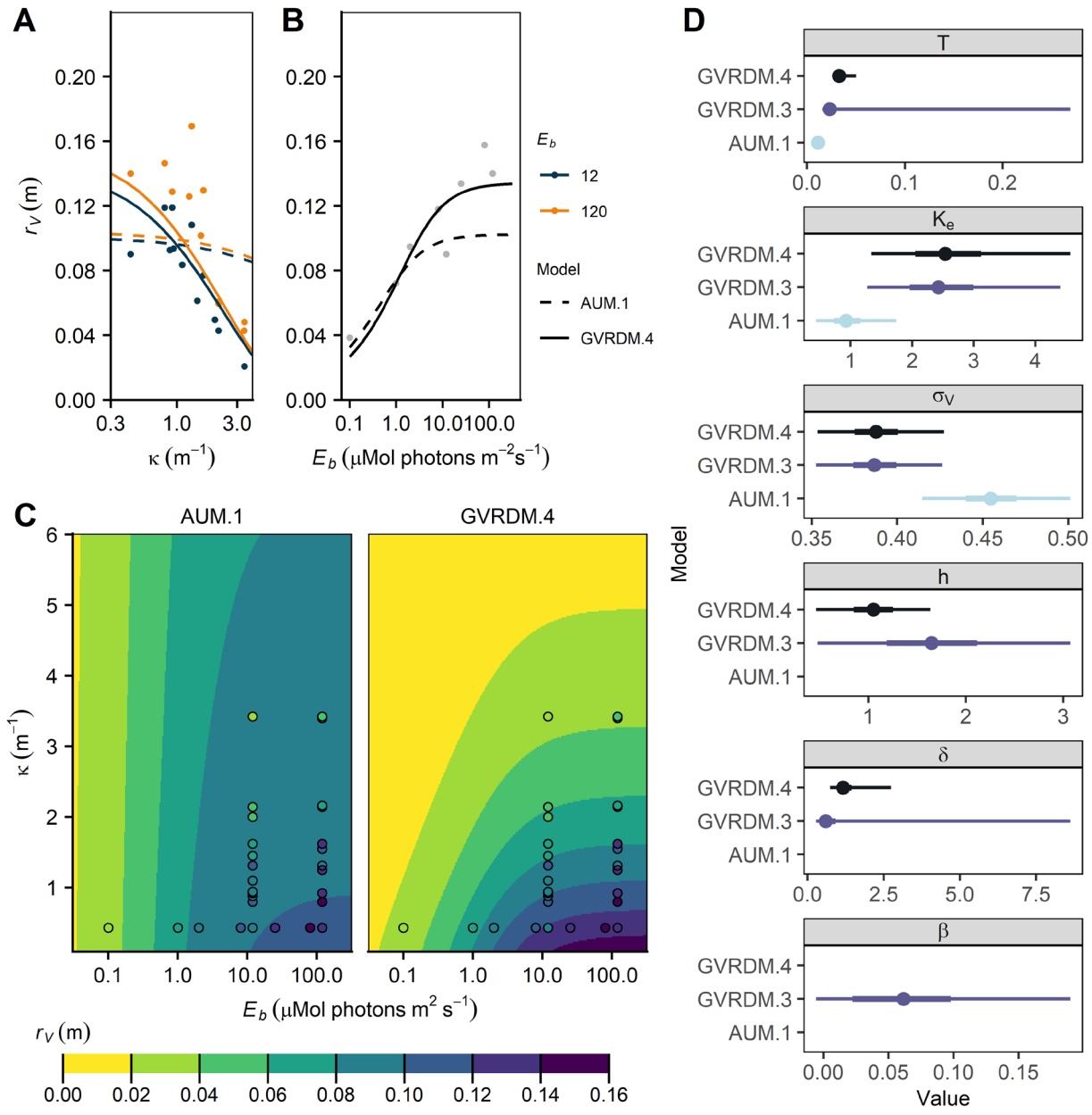

Figure 4. Case #2—Reaction distances for two-spotted goby reacting to ten *Calanus finmarchicus*, along a gradient of effective attenuation coefficient, κ, and light, E_b, for the Aksnes and Utne model (AUM.1) and generalized visual reaction distance model without a non-visual reaction or β (GVRDM.4). Panels: (A) fitted and observed reaction distance along a gradient of κ at two levels of E_b (12 and 120 μMol·photons·m^{-2}·s^{-1}); (B) fitted (lines) and mean reaction distances for treatment levels (points) along a gradient of E_b under constant κ = 0.43 m-1; (C) fitted reaction distance surfaces and mean reaction distances for treatment levels (points) where fill color shows reaction distance;

890 (D) parameter estimates for AUM.1, GVRDM.3, and GVRDM.4 where points denote the mean and thick and thin

891 lines denote the 50% and 95% confidence intervals, respectively.

892

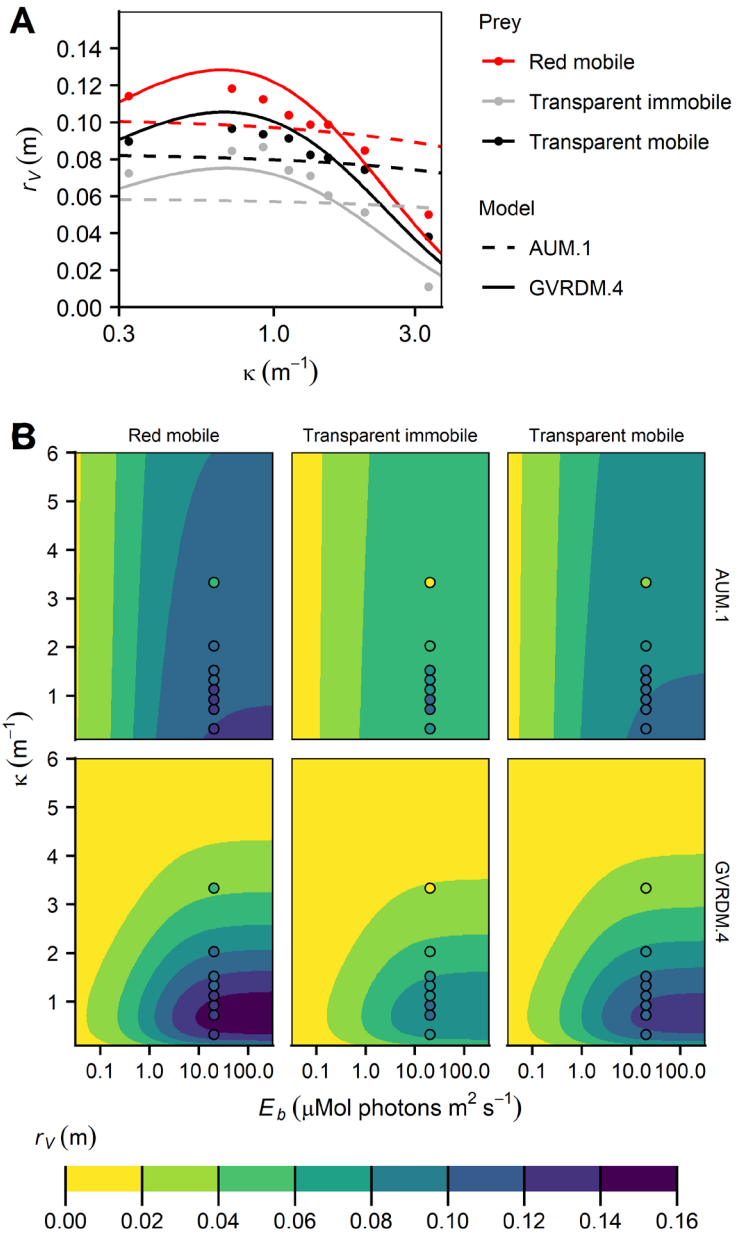
A
Prey
Red mobile
Transparent immobile
Transparent mobile
Model
AUM.1
GVRDM.4
r_V (m)
κ (m^{-1})
B
Red mobile
Transparent immobile
Transparent mobile
AUM.1
GVRDM.4
κ (m^{-1})
E_b (μMol photons m^2 s^{-1})
r_V (m)
C
T_{RM}
T_{TM}
T_{TI}
σ_V
h
δ
β
GVRDM.4
GVRDM.3
AUM.1
Model
Value

893

Figure 5. Case #3—Reaction distances for two-spotted goby reacting to single copepods, along gradients of light, E_b, and the effective attenuation coefficient, κ, for the Aksnes and Utne model (AUM.1) and the generalized visual reaction distance model without a non-visual reaction or β (GVRDM.4). Panels: (A) fitted (lines) and observed (points) reaction distances along a gradient of κ under constant E_b = 20 μMol·photons·m^{-2}·s^{-1}; (B) fitted reaction distance surfaces and mean reaction distances from experimental treatment levels (points) where fill color shows reaction distance, (C) parameter estimates for AUM.1, GVRDM.3, and GVRDM.4 where points denote the mean and thick and thin lines denote the 50% and 95% confidence intervals, respectively. Parameters for *Calanus finmarchicus/helgolandicus* prey are: T_{RM}—red mobile, T_{TI}—transparent immobile, and T_{TM}—transparent mobile.

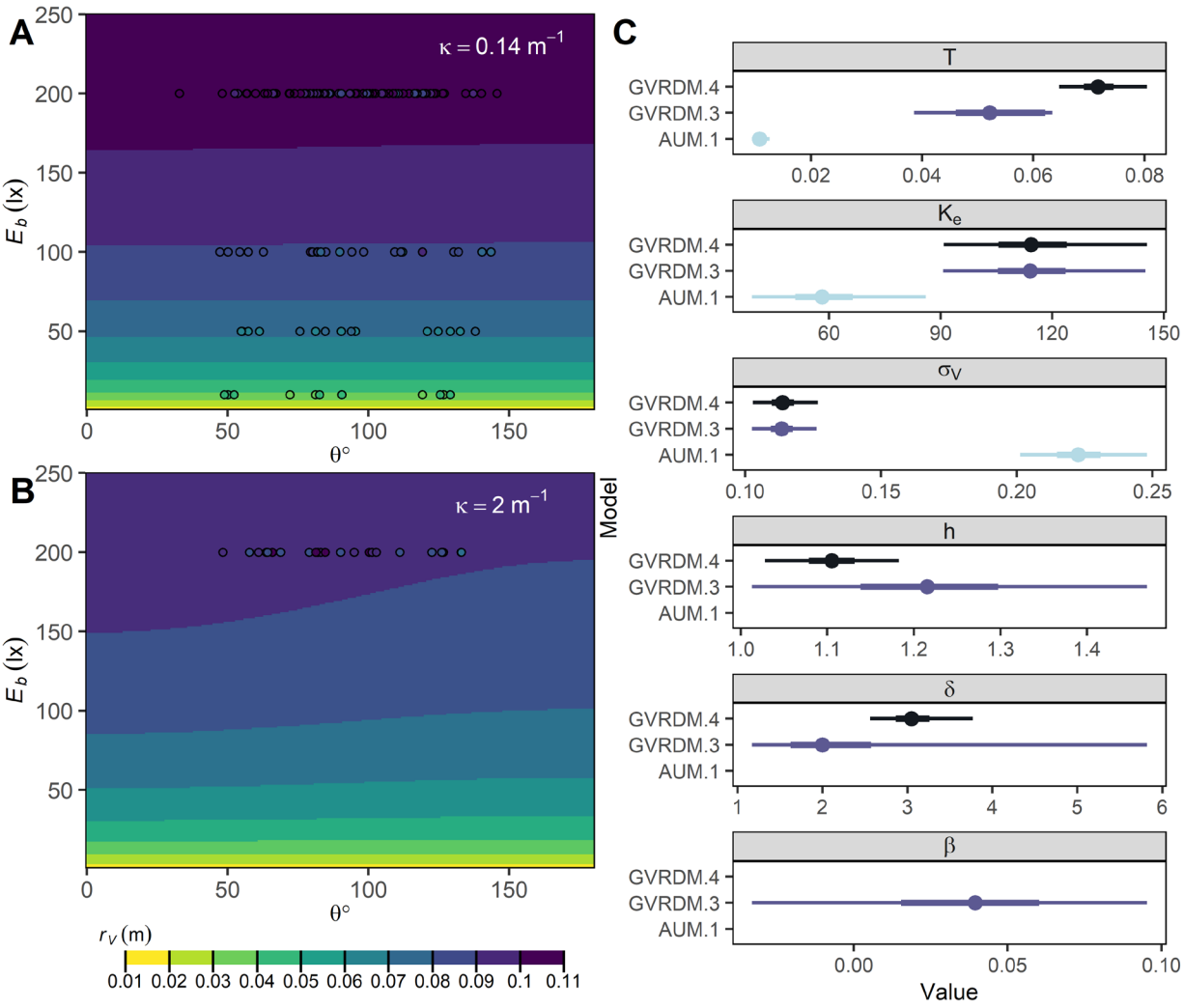

Figure 6. Case #4—Reaction distances and parameter estimates for stone moroko reacting to *Daphnia pulex*, as a function of light, E_b, and nadir viewing angle, θ. Panels show (A) reaction distance for effective attenuation coefficient, $\kappa = 0.14$ m^{-1}, for GVRDM.4, (B) reaction distances for $\kappa = 2$ m^{-1} for GVRDM.4, and (C) parameter estimates for AUM.1, GVRDM.3, and GVRDM.4. In panels A and B, colored surfaces shows the fit of the generalized visual reaction distance model without a non-visual reaction or β (GVRDM.4) and color-coded points denote observed reaction distances.

Merging empirical and mechanistic approaches to modeling aquatic visual foraging using a generalizable visual reaction distance model

Supplementary Material

Sean K. Rohan, David A. Beauchamp, Timothy E. Essington, Adam G. Hansen

Contents

Appendix A: Theoretical Basis

Contrast propagation

The physical dynamics of mechanistic models are derived from classic visibility theory (Duntley, 1952, 1948; Lythgoe, 1972; Middleton, 1952). In classic visibility theory, a target is visible to an observer if $C_T(r)$, the apparent contrast of a target at distance r, exceeds the minimum detectable contrast, C_{min}, of an observer's vision system (i.e. $C_T(r) > C_{min}$). Contrast is defined as the proportional difference in radiance between a target and background:

$$C_T = \frac{L_T - L_B}{L_B}, \tag{A1}$$

where L_T is radiance of the target, and L_B is radiance of the background. In classic visibility theory, the contrast of a target decreases with viewing distance, r (m), according to the law of contrast reduction (i.e. Koschmieder's law) as:

$$C_T(r) = C_T(0)\exp(-cr), \tag{A2}$$

where $C_T(r)$ is the apparent contrast of the target at distance r, $C_T(0)$ is contrast of the target at distance zero (i.e. inherent contrast), and c is beam attenuation (m^{-1}). Beam attenuation is the rate of attenuation of a collimated beam of light along a path, which occurs due to scattering and absorption (Kirk, 2011). Therefore, Eqn. A2 assumes that the only light that contributes to contrast propagation is light that travels along a direct path between the object and an observer (Duntley, 1952; Lee et al., 2015; Middleton, 1952; Preisendorfer, 1986).

The assumption of Eqn. A2 is valid if background and target radiances originate from positions that subtend a small angle relative to the resolution of the observer's visual field (Lee et al., 2015). In other words, Eqn. A2 is valid if the target can be treated as a point source (Duntley, 1952, 1948; Middleton, 1952). However, Eqn. A2 may not be valid in many underwater visibility applications because viewing distances are relatively short and forward-scattered light contributes to image propagation (Lee et al., 2015).

Following the radiative transfer equation, the radiance of a target at distance r is:

$$\frac{dL_T(r,\Theta,\lambda)}{dr} = -c(\lambda)L_T(r,\Theta,\lambda) + \int_{4\pi} L_T(r,\phi,\lambda)\beta(r,\phi,\lambda)d\Omega\,, \tag{A3}$$

and the radiance of a background reference location r', that is close to but does not overlap with the target, is:

$$\frac{dL_B(r',\Theta',\lambda)}{dr} = -c(\lambda)L_B(r',\Theta',\lambda) + \int_{4\pi} L_B(r',\phi,\lambda)\beta(r',\phi',\lambda)d\Omega\,. \tag{A4}$$

In Eqns. A3 and A4, Θ and Θ' are the three-dimensional directions between the observer and target, and observer and background, respectively, ϕ and ϕ' are directions towards the observer relative to Θ and Θ', Ω is an infinitesimal solid angle (steradians) oriented along ϕ or ϕ', and λ is wavelength. Conceptually, $-c(\lambda)L_T(r,\Theta,\lambda)$ and $-c(\lambda)L_B(r',\Theta',\lambda)$ represent losses of radiance along a path due to beam attenuation. The volume scattering functions, $\int_{4\pi} L_T(r,\phi,\lambda)\beta(r,\phi,\lambda)d\Omega$ and $\int_{4\pi} L_B(r',\phi,\lambda)\beta(r',\phi,\lambda)d\Omega$, represent radiance gained due to

forward scattering. The key assumption to derive the law of contrast reduction from the radiative transfer equation, it is that:

$$\int_{4\pi} L_T(r,\phi,\lambda)\beta(r,\phi,\lambda)d\Omega = \int_{4\pi} L_B(r',\phi,\lambda)\beta(r',\phi',\lambda)d\Omega\,, \tag{A5}$$

which is asymptotically true for a point source. Based on the assumption of Eqn. A5, the radiance difference between a target and background is:

$$L_T(r) - L_B(r') = \big(L_T(0) - L_B(0)\big)\exp(-cr)\,, \tag{A6}$$

which is equivalent to Eqn. A2. However, when a target cannot be considered a point source,

$$L_T(r) - L_B(r') = \big(L_T(0) - L_B(0)\big)\exp\big(-\big(c - \varepsilon b_f\big)r\big)\,, \tag{A7}$$

where b_f is the forward scattering coefficient (m^{-1}), and ε is a term that depends on L_T and L_B, and the distance between L_T and L_B (Lee et al., 2015). Expressed in terms of contrast:

$$C_a = C_0\exp\big(-\big(c - \varepsilon b_f\big)r\big)\,. \tag{A8}$$

Unfortunately, there is no generalizable value of ε; ε→1 when the target is large, while for a point source, ε→0 (Lee et al., 2015).

Contrast reduction following Eqn. A8 instead of Eqn. A2 has implications for visual reaction distance experiments and mechanistic encounter distance models. To satisfy Eqn. A2, some studies have emphasized the importance of deriving beam attenuation, *c*, from transmittance measurements that minimize or are adjusted to minimize contributions of forward scattered light, to avoid underestimating beam attenuation (e.g. Utne-Palm 1999; Meager et al. 2005). To fit their model to data from a visual foraging experiment, Aksnes and Utne (1997) adjusted spectrophotometer absorbance measurements to derive values of beam attenuation that were corrected to omit contributions of forward-scattered light to spectrophotometer measurements, following Zaneveld et al. (1979). However, based on Eqn. A8, omitting forward-scattering would underestimate contrast propagation.

Naka-Rushton function

Aksnes and Utne (1997) used a Michaelis-Menten function to represent the light intensity-response of a fish vision system, based on the suggestion by Cornsweet (1970) that such a functional form provides a generic representation of the retinal-neural intensity response of the vertebrate vision system to light, rather than being an explicit representation of a mechanism. However, a Michaelis-Menten function is equivalent to the Naka-Rushton function that characterizes the light intensity-response of horizontal cells of vertebrate retina (Naka et al., 1988; Naka and Rushton, 1966a, 1966b). In the Naka-Rushton function,

$$V = \frac{V_{max} I^{\alpha}}{I_{50}^{\alpha} + I^{\alpha}} + V_0, \tag{A9}$$

V is the membrane voltage potential (mV) that is stimulated by light intensity I, V_{max} is the maximum induced voltage potential (mV), V_0 is resting potential (mV), I_{50} is a half-saturation level, and α is a slope parameter (Naka et al., 1988; Naka and Rushton, 1966a). For vertebrates, retinal-neural intensity-response relationships can often be approximated using the Naka-Rushton function assuming $\alpha = 1$ and $V_0 = 0$.

The functional representation of the Naka-Rushton function for scaling the visual response is related to the contrast propagation assumption of the Aksnes and Utne model as follows. In the fish retinae, horizontal cells receive inputs from photoreceptors, interplexiform cells, and other horizontal cells (Djamgoz and Yamada, 1990; Kaneko, 1971). Coupled horizontal cells of the same type integrate across inputs and functionally 'measure' ambient

illumination (Djamgoz and Yamada, 1990). This is important because the absolute intensity-response of the vision system to a response scales incrementally with the adapting level of ambient illumination (Naka et al., 1979; Sakai et al., 1995). The contrast propagation function of the Aksnes and Utne model assumes that contrast scales in constant proportion with background illumination (i.e. contrast remains constant regardless of light levels). Thus, in the Aksnes and Utne model, the Naka-Rushton function scales the incremental absolute sensitivity of the vision system to a stimulus of constant contrast across varying levels of light intensity. These mechanisms of adaptation and intensity-response are more proximal in the neural-retinal pathway than quantum integration by photoreceptors that can overestimate visual range in the absence of outside constraints on contrast sensitivity (e.g. Ruxton and Johnsen, 2016).

Appendix B: Data sources, preparation, code, and model-fitting

Screening predator-prey reaction distance experiments

We reviewed every visual predator-prey experimental study we are aware of and evaluated whether they were suitable for model fitting and evaluation in our study based on eight criteria (Table B1). Criteria #1–5 were essential for model fitting in our study. Criteria #6–8 were desirable for evaluating model performance but not essential for specific cases if criteria #1–5 were met. Our review included every published visual predator-prey experiment we were aware of that reported reaction distances of fish to prey under varying conditions in the visual environment were manipulated for experimental treatments (Table B2). Aside from our screening criteria (Table B1), we aimed to include at least one case where there was evidence of a non-visual reaction at low light levels (based on the authors' description in the text, visual examination of figures, and the structure of empirical models fitted to the experimental data, at least one piscivore case, at least one planktivore case, and at least one case where reaction angles were recorded during experiments.

The 32 studies we reviewed included 59 predator-prey systems of which 96.7% (57/59) had data we could either directly access (10/59) or digitize from figures (47/59; Table B3). Of the systems where we could obtain data, 31.6% (18/57) manipulated light and turbidity or could be combined with other experiments to fill gaps from a single study (Criteria #1; Table B3). We note that in *Appendix G: Asymptotic equivalence between behavioral and theoretical models*, we examine the link between empirical models reported from light-treatment-only systems and mechanistic relationships that are used in the Aksnes and Utne model and generalized visual reaction distance model. Fourteen (14) out of 18 remaining systems included measurements of absorbance or beam attenuation, or manipulated turbidity using suspendoids and reported turbidity units in a manner that would allow post hoc estimation of beam attenuation/effective attenuation coefficient using conversions reported in the literature (Criteria #2; Table B3). Among the 14 remaining predator-prey systems, Confer et al. (1978) did not manipulate or report light and turbidity simultaneously for a lean lake trout-cladoceran system (Criteria #1), Meager et al. (2005) did not have a sufficient sample size for Atlantic cod-mysid system (Criteria #3), and Utne (1997) did not have sufficient dynamic range of variation in light treatments for two-spotted goby reacting to individual *Calanus finmarchicus*/*Calanus helgolandicus* to fit models to data (Criteria #4), leaving eleven predator-prey systems that met our criteria for consideration in cases (Table B3). We now discuss the remaining predator-prey systems (seven piscivore, four planktivore).

The seven remaining studies that reported results of piscivore experiments were conducted using similar experimental protocols and considered a similar suite of empirical models to fit to experimental data (Hansen et al., 2013; Mazur and Beauchamp, 2003; Vogel and Beauchamp, 1999). However, only Hansen et al. (2013) reported a relationship between experimentally measured nephelometric turbidity units (NTU) and absorbance (as a proxy for beam attenuation; Criteria #2). Plots and models from Hansen et al. (2013) provided some indication that non-visual reaction may have occurred during experimental trials (Criteria #5), and we had access to original data to facilitate direct comparison with best-fit empirical models

(Criteria #8). We therefore selected Hansen et al. (2013) as a piscivore case (subsection 2.4.1 Case #1—Piscivore reacting to fish prey) to minimize potential uncertainty associated with conversions from the literature.

Among the four zooplanktivore systems, three used the same predator and prey species and measurements were obtained using similar experimental protocols (Utne-Palm, 1999; Utne, 1997). One of the systems (two-spotted goby reacting to 10 *Calanus finmarchicus/helgolandicus*) was used as an example in Aksnes and Utne (1997) and parameters from the system have been used in numerous visual foraging model applications (e.g. Langbehn and Varpe 2017) and, we used the system for *Case #2—Planktivore reacting to a group of ten zooplankton prey* (subsection 2.4.2). Utne-Palm (1999) reported results for three predator-prey systems, each of which used two-spotted goby as the predator, but only manipulated turbidity and not light levels (Criteria #1). We determined that it would be feasible to estimate parameters for the predator-prey systems from Utne-Palm (1999) if parameter estimates from Case #2 could be transferred. Thus, we used the three predator-prey systems from Utne-Palm (1999; predator: two-spotted goby, prey: transparent mobile, transparent immobile, and red mobile *C. finmarchicus/helgolandicus*) for *Case #3—Planktivore reacting to a single zooplankton prey* (subsection 2.4.3).

The final zooplanktivore system, stone moroko reacting to *Daphnia pulex*, was the only system where nadir viewing angle at the point of reaction was reported along with reaction distance (Asaeda et al., 2002; Criteria #6). The study did not report a relationship between turbidity measurements presented for the experiments (nephelometric turbidity units) generated using kaolinite and physically interpretable attenuation coefficients. However, relationships between NTU and beam attenuation/absorption have been reported in the literature. Therefore, we used the stone moroko-*Daphnia pulex* system for *Case #4—Planktivore reacting to single zooplankton, with angular dependence* (subsection 2.4.4).

Table B1. Criteria for selecting predator-prey cases for our study.

#	Criteria	Rationale
1	Did experiments manipulate both light and turbidity?	The generalized visual reaction distance model and Aksnes and Utne model is fitted to light and turbidity data.
2	Were beam attenuation or absorbance measured? If not, is a reasonable conversion available for experimental units (e.g. conversion from NTU to beam attenuation for bentonite)?	The generalized visual reaction distance model and Aksnes and Utne model characterize the transmission of light through water based on physically interpretable attenuation coefficients (beam attenuation, effective attenuation coefficient, and diffuse attenuation coefficient). Nephelometric turbidity units (NTU) must be converted to directly characterize light attenuation.
3	Were sample sizes large enough for model fitting?	Available sample sizes should be adequate for model-fitting given the number of parameters estimated in each model. Models and number of parameters (in parenthesis): AUM.1 (3); AUM.2 (6); GVRDM.1 (9); GVRDM.2 (8); GVRDM.3 (6); GVRDM.4 (5)
4	Was the dynamic range of treatment levels sufficient?	Experimental treatments need to span a sufficient absolute and dynamic range for model-fitting.
5	Was there evidence of a visual reaction?	Visual encounter distance models are not appropriate for cases where predators use senses other than vision are used for prey detection.
6	Were reaction angles measured?	We sought to include at least one case where reaction angles were reported in order to evaluate if information about reaction angle improved model fit.
7	Was there evidence of non-visual reaction at low light levels?	We sought to include at least one case where a non-visual reaction may have occurred at low light levels.
8	Direct access to the original data?	Fitting the model to original data allows direct comparison between the GVRDM, AUM, and and best-fit empirical models from visual foraging experiments.

Table B2. Visual encounter distance experiments reviewed. Columns show predator and prey treatments, measurements reported for reaction distance (*r*), light, and turbidity, the suspendoid used (Susp.), availability of a conversion to beam attenuation or absorption (Conv.; Y = Yes, reported or conversion measured by authors; N = No; Ext. = External, conversion available in the literature), nadir viewing angle reported (Y = Yes, N = No); sample size available as either the original data set or digitization of data from plots (n), source. Dashes (-) indicate no treatment or that data were not collected or reported by the authors.

		Measurement units							
Predator	Prey	*r*	Light	Turbidity	Susp.	Conv.	θ	n	Source
stone moroko, *Pseudorasbora parva*	**cladoceran *Daphnia pulex***	**body length**	**lx**	**NTU**	**kaolinite**	**Ext.**	**Y**	**209**	Asaeda et al. (2002)
rainbow trout, *Oncorhynchus mykiss*	mealworm	cm	-	NTU	Stream sediment	No	N	57	Barrett et al. (1992)
bluegill, *Lepomis macrochirus*	cladoceran *Daphnia galeata mendotae*	cm	PFD	-	-	-	N	3	Breck and Gitter (1983)
bluegill, *Lepomis macrochirus*	cladoceran *Daphnia magna*	cm	PFD	-	-	-	N	8	Breck and Gitter (1983)
bay anchovy *Anchoa mitchilli*	brine shrimp (nauplii) *Artemia* sp.	mm	lx	-	-	-	N	51	Chesney (2008)
bay anchovy *Anchoa mitchilli*	brine shrimp (nauplii) *Artemia* sp.	body length	lx	-	-	-	Y	42	Chesney (2008)
bay anchovy *Anchoa mitchilli*	L-rotifer	mm	lx	NTU	algae (*Isochyris galbana*)	N	N	145	Chesney (2008)
brook trout *Salvelinus fontinalis*	cladoceran *Daphnia pulex*	cm	lx	-	-	-	N	9	Confer et al. (1978)
lean lake trout *Salvelinus namaycush*	cladoceran *Daphnia magna*	cm	lx	-	-	-	N	29	Confer et al. (1978)
lean lake trout *Salvelinus namaycush*	cladoceran *Daphnia magna*	cm	lx	absorbance m^{-1}	Green clay	No	N	8	Confer et al. (1978)
pumpkinseed *Lepomis gibbosus*	cladoceran *Daphnia pulex*	cm	lx	-	-	-	N	11	Confer et al. (1978)

		Measurement units							
Predator	Prey	*r*	Light	Turbidity	Susp.	Conv.	*θ*	n	Source
largemouth bass *Micropterus salmoides*	crayfish (moving)	cm	lx	JTU	bentonite	Ext.	N	107	Crowl (1989)
largemouth bass *Micropterus salmoides*	crayfish (not moving)	cm	lx	JTU	bentonite	Ext.	N	410	Crowl (1989)
Chinook salmon *Oncorhynchus tshawytscha*	brine shrimp *Artemia salina*	cm	PFD	NTU	marsh sediment	N	N	14	Gregory and Northcote (1993)
Chinook salmon *Oncorhynchus tshawytscha*	coastal cutthroat trout *Oncorhynchus clarkia clarkii*	cm	lx	NTU	-	Y	N	73*	Hansen et al. (2013)
Chinook salmon *Oncorhynchus tshawytscha*	**rainbow trout *Oncorhynchus mykiss***	**cm**	**lx**	**NTU**	**kaolin**	**Y**	**N**	**629***	**Hansen et al. (2013)**
coastal cutthroat trout *Oncorhynchus clarkii clarkii*	rainbow trout *Oncorhynchus mykiss*	cm	lx	NTU	-	-	N	269*	Hansen et al. (2013)
coastal cutthroat trout *Oncorhynchus clarkii clarkii*	threespine stickleback *Gasterosteus aculeatus*	cm	lx	NTU	-	-	N	70*	Hansen et al. (2013)
Cape silverside *Atherina breviceps*	cladoceran *Daphnia* sp.	cm	-	NTU	Estuarine silt	N	N	4	Hecht and van der Lingen (1992)
coastal cutthroat trout *Oncorhynchus clarkii clarkii*	copepod *Diaptomus kenai*	cm	PFD	-	-	-	N	5	Henderson and Northcote (1985)

		Measurement units							
Predator	Prey	*r*	Light	Turbidity	Susp.	Conv.	θ	n	Source
coastal cutthroat trout *Oncorhynchus clarkii clarkii*	food pellets	cm	PFD	-	-	-	N	5	Henderson and Northcote (1985)
Dolly Varden trout *Salvelinus malma*	copepod *Diaptomus kenai*	cm	PFD	-	-	-	N	6	Henderson and Northcote (1985)
Dolly Varden trout *Salvelinus malma*	food pellets	cm	PFD	-	-	-	N	6	Henderson and Northcote (1985)
lean lake trout *Salvelinus namaycush*	amphipod (stationary) *Hyalella azteca*	cm	PFD	-	-	-	N	6	Holbrook et al. (2013)
lean lake trout *Salvelinus namaycush*	amphipod (moving) *Hyalella azteca*	cm	PFD	-	-	-	N	6	Holbrook et al. (2013)
lean lake trout *Salvelinus namaycush*	cladoceran *Daphnia magna*	cm	PFD	-	-	-	N	6	Holbrook et al. (2013)
lean lake trout *Salvelinus namaycush*	mysid (moving) *Mysis diluviana*	cm	PFD	-	-	-	N	6	Holbrook et al. (2013)
lean lake trout *Salvelinus namaycush*	mysid (stationary) *Mysis diluviana*	cm	PFD	-	-	-	N	6	Holbrook et al. (2013)
largemouth bass *Micropterus salmoides*	redside shiner *Richardsonius balteatus*	cm	lx	-	-	-	N	0	Howick and O'Brien (1983)
largemouth bass *Micropterus salmoides*	bluegill *Lepomis macrochirus*	cm	lx	-	-	-	N	0	Howick and O'Brien (1983)

		Measurement units							
Predator	Prey	*r*	Light	Turbidity	Susp.	Conv.	θ	n	Source
pike *Esox lucius*	cladoceran *Daphnia* sp.	cm	-	Other	algae, dissolved organic matter	N	-	3	Jönsson et al. (2012)
pike *Esox lucius*	roach *Rutilus rutilus*	cm	-	Other	algae, dissolved organic matter	N	-	3	Jönsson et al. (2012)
siscowet lake trout *Salvelinus namaycush siscowet*	golden shiner *Notemigonus crysoleucas*	cm	PFD	-	-	-	N	6	Keyler et al. (2015)
siscowet lake trout *Salvelinus namaycush siscowet*	golden shiner (large) *Notemigonus crysoleucas*	cm	PFD	-	-	-	N	6	Keyler et al. (2015)
siscowet lake trout *Salvelinus namaycush siscowet*	golden shiner (moving) *Notemigonus crysoleucas*	cm	PFD	-	-	-	N	6	Keyler et al. (2015)
siscowet lake trout *Salvelinus namaycush siscowet*	golden shiner (small) *Notemigonus crysoleucas*	cm	PFD	-	-	-	N	6	Keyler et al. (2015)
siscowet lake trout *Salvelinus namaycush siscowet*	golden shiner (stationary) *Notemigonus crysoleucas*	cm	PFD	-	-	-	N	4	Keyler et al. (2015)
siscowet lake trout *Salvelinus namaycush siscowet*	deepwater sculpin *Myoxocephalus thompsonii*	cm	PFD	-	-	-	N	15	Keyler et al. (2019)

		Measurement units							
Predator	Prey	*r*	Light	Turbidity	Susp.	Conv.	θ	n	Source
lake herring *Coregonus artedi*	copepod *Limnocalanus macrurus*	cm	lx	-	-	-	Y	8	Link and Edsall (1996)
cutthroat trout *O. clarkii clarkia*	cutthroat trout *O. clarkii clarkii*	cm	lx	NTU	bentonite	Ext.	N	174*	Mazur and Beauchamp (2003)
cutthroat trout *O. clarkii clarkii*	rainbow trout *Oncorhynchus mykiss*	cm	lx	NTU	bentonite	Ext.	N	369*	Mazur and Beauchamp (2003)
lake trout *Salvelinus namaycush*	cutthroat trout *O. clarkii clarkii*	cm	lx	NTU	bentonite	Ext.	N	263*	Mazur and Beauchamp (2003)
lake trout *Salvelinus namaycush*	rainbow trout *Oncorhynchus mykiss*	cm	lx	NTU	bentonite	Ext.	N	92*	Mazur and Beauchamp (2003)
rainbow trout *Oncorhynchus mykiss*	cutthroat trout *O. clarkii clarkii*	cm	lx	NTU	bentonite	Ext.	N	111*	Mazur and Beauchamp (2003)
rainbow trout *Oncorhynchus mykiss*	rainbow trout *Oncorhynchus mykiss*	cm	lx	NTU	bentonite	Ext.	N	155*	Mazur and Beauchamp (2003)
Atlantic cod *Gadus morhua*	mysid *Praunus neglectus*	cm	PFD	-	-	-	N	5	Meager et al. (2010)
Atlantic cod *Gadus morhua*	mysid *Praunus neglectus*	cm	PFD	absorbance m^{-1}	kaolin	Y	N	5	Meager et al. (2005)
emerald shiner *Notropis atherinoides*	cladoceran *Daphnia magna*	cm	-	NTU	emulsified spinach, lake mud	N	N	7	Nieman and Gray (2019)

		Measurement units							
			Ligh			Con			
Predator	Prey	*r*	t	Turbidity	Susp.	v.	θ	n	Source
walleye *Sander vitreus*	emerald shiner *Notropis atherinoides*	cm	-	NTU	emulsified spinach, lake mud	N	N	4	Nieman and Gray (2019)
walleye *Sander vitreus*	golden shiner *Notemigonus crysoleucas*	cm	-	NTU	emulsified spinach, lake mud	N	N	7	Nieman and Gray (2019)
threespine stickleback *Gasterosteus aculeatus*	brine shrimp *Artemia salina*	cm	-	NTU	bentonite	Ext.	N	4	Quesenberry et al. (2007)
pike *Esox lucius*	roach *Rutilus rutilus*	cm	-	Other	algae, humic substance, clay	N	N	3	Ranåker et al. (2012)
yellow perch *Perca flavescens*	cladoceran *Daphnia pulicaria*	cm	lx	-	-	-	N	13	Richmond et al. (2004)
Miry's demoiselle *Neopomacentrus miryae*	brine shrimp *Artemia salina*	cm	lx	-	-	-	N	14	Rickel and Genin (2005)
Arctic grayling *Thymallus arcticus*	cladoceran *Bosmina longirostris*	cm	lx	-	-	-	N	18	Schmidt and O'Brien (1982)
Arctic grayling *Thymallus arcticus*	copepod *Cyclops scutifer*	cm	lx	-	-	-	N	19	Schmidt and O'Brien (1982)
Arctic grayling *Thymallus arcticus*	cladoceran *Daphnia longiremis*	cm	lx	-	-	-	N	41	Schmidt and O'Brien (1982)
Arctic grayling *Thymallus arcticus*	cladoceran *Daphnia pulex*	cm	lx	-	-	-	N	26	Schmidt and O'Brien (1982)

		Measurement units							
Predator	Prey	*r*	Light	Turbidity	Susp.	Conv.	θ	n	Source
Arctic grayling *Thymallus arcticus*	copepod *Heterocope septentrionalis*	cm	lx	-	-	-	N	71	Schmidt and O'Brien (1982)
flavescent peacock *Aulonocara stuartgranti*	brine shrimp *Artemia* sp. (dead)	cm	PFD	-	-	-	N	5	Schwalbe and Webb (2015)
flavescent peacock *Aulonocara stuartgranti*	brine shrimp *Artemia* sp. (living)	cm	PFD	-	-	-	N	5	Schwalbe et al. (2015)
Tramitichromis sp.	brine shrimp *Artemia* sp. (dead)	cm	PFD	-	-	-	N	5	Schwalbe et al. (2015)
Tramitichromis sp.	brine shrimp *Artemia* sp. (living)	cm	PFD	-	-	-	N	5	Schwalbe et al. (2015)
brook trout *Salvelinus fontinalis*	housefly *Musca domestica*	cm	lx	NTU	riparian soil	-	N	39	Sweka and Hartman (2001)
smallmouth bass *Micropterus dolomieu*	housefly *Musca domestica*	cm	lx	NTU	riparian soil	-	N	54	Sweka and Hartman (2003)
two-spotted goby *Gobius flavescens*	**copepod (red mobile) *Calanus finmarchicus* *C. helgolandicus***	**cm**	**PFD**	**absorbance m^{-1}**	**Diatomaceous earth**	**Yes**	**N**	**8**	**Utne-Palm (1999)**
two-spotted goby *Gobius flavescens*	**copepod (transparent immobile) *Calanus finmarchicus* *C. helgolandicus***	**cm**	**PFD**	**absorbance m^{-1}**	**Diatomaceous earth**	**Yes**	**N**	**8**	**Utne-Palm (1999)**

		Measurement units							
Predator	Prey	*r*	Light	Turbidity	Susp.	Conv.	θ	n	Source
two-spotted goby *Gobius flavescens*	**copepod (transparent mobile) *Calanus finmarchicus* *C. helgolandicus***	**cm**	**PFD**	**absorbance m^{-1}**	**Diatomaceous earth**	**Yes**	**N**	**8**	**Utne-Palm (1999)**
two-spotted goby *Gobius flavescens*	copepod (10 prey) *Acartia clausi*	cm	PFD	absorbance m^{-1}	-	-	N	51	Utne (1997)
two-spotted goby *Gobius flavescens*	copepod (1 prey) *Calanus finmarchicus*	cm	PFD	absorbance m^{-1}	Diatomaceous earth	Yes	N	81	Utne (1997)
two-spotted goby *Gobius flavescens*	**copepod (10 prey) *Calanus finmarchicus***	**cm**	**PFD**	**absorbance m^{-1}**	**Diatomaceous earth**	**Yes**	**N**	**214**	**Utne (1997)**
bluegill *Lepomis macrochirus*	cladoceran *Daphnia pulex*	cm	lx	JTU	Pond sediment	No	N	57	Vinyard and O'Brien (1976)
lake trout *Salvelinus namaycush*	cutthroat trout *O. clarkii clarkii*	cm	lx	NTU	bentonite	Ext.	N	648*	Vogel and Beauchamp (1999)
lake trout *Salvelinus namaycush*	rainbow trout *Oncorhynchus mykiss*	cm	lx	NTU	bentonite	Ext.	N	1,321*	Vogel and Beauchamp (1999)

*—Original data from experiments were available. Sample size indicates number of individual reactions.

Table B3. Evaluation of cases based on screening criteria. Cases selected for our study are shown in bold.

Predator	Prey	Criteria								Source
		1	2	3	4	5	6	7	8	
stone moroko, *Pseudorasbora parva*	**cladoceran *Daphnia pulex***	**Y**	**Y**	**Y**	**Y**	**Y**	**Y**	**N**	**N**	**Asaeda et al. (2002)**
rainbow trout, *Oncorhynchus mykiss*	mealworm	N	N	Y	N	Y	N	N	N	Barrett et al. (1992)
bluegill, *Lepomis macrochirus*	cladoceran *Daphnia galeata mendotae*	N	N	Y	N	Y	N	N	N	Breck and Gitter (1983)
bluegill, *Lepomis macrochirus*	cladoceran *Daphnia magna*	N	N	Y	N	Y	N	N	N	Breck and Gitter (1983)
bay anchovy *Anchoa mitchilli*	brine shrimp (nauplii) *Artemia* sp.	N	N	Y	N	Y	N	N	N	Chesney (2008)
bay anchovy *Anchoa mitchilli*	brine shrimp (nauplii) *Artemia* sp. L-rotifer	N	N	Y	N	Y	Y	N	N	Chesney (2008)
bay anchovy *Anchoa mitchilli*	L-rotifer	Y	N	Y	N	Y	N	N	N	Chesney (2008)
brook trout *Salvelinus fontinalis*	cladoceran *Daphnia pulex*	N	N	Y	N	Y	N	N	N	Confer et al. (1978)
lean lake trout *Salvelinus namaycush*	cladoceran *Daphnia magna*	N	N	Y	N	Y	N	N	N	Confer et al. (1978)
lean lake trout *Salvelinus namaycush*	cladoceran *Daphnia magna*	Y	N	Y	N	Y	N	N	N	Confer et al. (1978)
pumpkinseed *Lepomis gibbosus*	cladoceran *Daphnia pulex*	N	N	Y	N	Y	N	N	N	Confer et al. (1978)
largemouth bass *Micropterus salmoides*	crayfish (moving)	N	Y	Y	N	Y	N	N	N	Crowl (1989)
largemouth bass *Micropterus salmoides*	crayfish (not moving)	N	Y	Y	N	Y	N	N	N	Crowl (1989)

Predator	Prey	Criteria								Source
		1	2	3	4	5	6	7	8	
Chinook salmon *Oncorhynchus tshawytscha*	brine shrimp *Artemia salina*	N	N	Y	N	Y	N	N	N	Gregory and Northcote (1993)
Chinook salmon *Oncorhynchus tshawytscha*	coastal cutthroat trout *Oncorhynchus clarkia clarkii*	N	Y	Y	N	Y	N	U	Y	Hansen et al. (2013)
Chinook salmon *Oncorhynchus tshawytscha*	**rainbow trout *Oncorhynchus mykiss***	**Y**	**Y**	**Y**	**Y**	**Y**	**N**	**U**	**Y**	**Hansen et al. (2013)**
coastal cutthroat trout *Oncorhynchus clarkii clarkii*	rainbow trout *Oncorhynchus mykiss*	N	Y	Y	N	Y	N	U	Y	Hansen et al. (2013)
coastal cutthroat trout *Oncorhynchus clarkii clarkii*	threespine stickleback *Gasterosteus aculeatus*	N	Y	Y	N	Y	N	U	Y	Hansen et al. (2013)
Cape silverside *Atherina breviceps*	cladoceran *Daphnia* sp.	N	N	N	N	Y	N	N	N	Hecht and van der Lingen (1992)
coastal cutthroat trout *Oncorhynchus clarkii clarkii*	copepod *Diaptomus kenai*	N	N	N	N	Y	N	N	N	Henderson and Northcote (1985)
coastal cutthroat trout *Oncorhynchus clarkii clarkii*	food pellets	N	N	N	N	Y	N	N	N	Henderson and Northcote (1985)
Dolly Varden trout *Salvelinus malma*	copepod *Diaptomus kenai*	N	N	N	N	Y	N	N	N	Henderson and Northcote (1985)
Dolly Varden trout *Salvelinus malma*	food pellets	N	N	N	N	Y	N	N	N	Henderson and Northcote (1985)
lean lake trout *Salvelinus namaycush*	amphipod (stationary) *Hyalella azteca*	N	N	N	N	N	N	Y	N	Holbrook et al. (2013)

Predator	Prey	Criteria								Source
		1	2	3	4	5	6	7	8	
lean lake trout *Salvelinus namaycush*	amphipod (moving) *Hyalella azteca*	N	N	N	N	N	N	Y	N	Holbrook et al. (2013)
lean lake trout *Salvelinus namaycush*	cladoceran *Daphnia magna*	N	N	N	N	Y	N	N	N	Holbrook et al. (2013)
lean lake trout *Salvelinus namaycush*	mysid (moving) *Mysis diluviana*	N	N	N	N	U	N	U	N	Holbrook et al. (2013)
lean lake trout *Salvelinus namaycush*	mysid (stationary) *Mysis diluviana*	N	N	N	N	U	N	U	N	Holbrook et al. (2013)
largemouth bass *Micropterus salmoides*	redside shiner *Richardsonius balteatus*	N	N	N	N	Y	N	N	N	Howick and O'Brien (1983)
largemouth bass *Micropterus salmoides*	bluegill *Lepomis macrochirus*	N	N	N	N	Y	N	N	N	Howick and O'Brien (1983)
pike *Esox lucius*	cladoceran *Daphnia* sp.	N	N	N	N	Y	N	N	N	Jönsson et al. (2012)
pike *Esox lucius*	roach *Rutilus rutilus*	N	N	N	N	Y	N	N	N	Jönsson et al. (2012)
siscowet lake trout *Salvelinus namaycush siscowet*	golden shiner *Notemigonus crysoleucas*	N	N	Y	N	Y	N	N	N	Keyler et al. (2015)
siscowet lake trout *Salvelinus namaycush siscowet*	golden shiner (large) *Notemigonus crysoleucas*	N	N	Y	N	Y	N	N	N	Keyler et al. (2015)
siscowet lake trout *Salvelinus namaycush siscowet*	golden shiner (moving) *Notemigonus crysoleucas*	N	N	Y	N	Y	N	N	N	Keyler et al. (2015)
siscowet lake trout *Salvelinus namaycush siscowet*	golden shiner (small) *Notemigonus crysoleucas*	N	N	Y	N	Y	N	N	N	Keyler et al. (2015)

Predator	Prey	Criteria								Source
		1	2	3	4	5	6	7	8	
siscowet lake trout *Salvelinus namaycush siscowet*	golden shiner (stationary) *Notemigonus crysoleucas*	N	N	Y	N	Y	N	N	N	Keyler et al. (2015)
siscowet lake trout *Salvelinus namaycush siscowet*	deepwater sculpin *Myoxocephalus thompsonii*	N	N	Y	N	Y	N	N	N	Keyler et al. (2019)
lake herring *Coregonus artedi*	copepod *Limnocalanus macrurus*	N	N	Y	N	Y	Y	N	N	Link and Edsall (1996)
cutthroat trout *O. clarkii clarkia*	cutthroat trout *O. clarkii clarkii*	Y	Y	Y	Y	Y	N	U	Y	Mazur and Beauchamp (2003)
cutthroat trout *O. clarkii clarkii*	rainbow trout *Oncorhynchus mykiss*	Y	Y	Y	Y	Y	N	U	Y	Mazur and Beauchamp (2003)
lake trout *Salvelinus namaycush*	cutthroat trout *O. clarkii clarkii*	Y	Y	Y	Y	Y	N	U	Y	Mazur and Beauchamp (2003)
lake trout *Salvelinus namaycush*	rainbow trout *Oncorhynchus mykiss*	Y	Y	Y	Y	Y	N	U	Y	Mazur and Beauchamp (2003)
rainbow trout *Oncorhynchus mykiss*	cutthroat trout *O. clarkii clarkii*	Y	Y	Y	Y	Y	N	U	Y	Mazur and Beauchamp (2003)
rainbow trout *Oncorhynchus mykiss*	rainbow trout *Oncorhynchus mykiss*	Y	Y	Y	Y	Y	N	U	Y	Mazur and Beauchamp (2003)
Atlantic cod *Gadus morhua*	mysid *Praunus neglectus*	N	N	N	N	Y	N	U	N	Meager et al (2010)

Predator	Prey	Criteria								Source
		1	2	3	4	5	6	7	8	
Atlantic cod *Gadus morhua*	mysid *Praunus neglectus*	N	Y	N	N	Y	N	U	N	Meager et al. (2005)
emerald shiner *Notropis atherinoides*	cladoceran *Daphnia magna*	N	N	Y	N	Y	N	N	N	Nieman and Gray (2018)
walleye *Sander vitreus*	emerald shiner *Notropis atherinoides*	N	N	N	N	Y	N	N	N	Nieman and Gray (2018)
walleye *Sander vitreus*	golden shiner *Notemigonus crysoleucas*	N	N	N	N	Y	N	N	N	Nieman and Gray (2018)
threespine stickleback *Gasterosteus aculeatus*	brine shrimp *Artemia salina*	N	Y	N	N	Y	N	N	N	Quesenberry et al. (2007)
pike *Esox lucius*	roach *Rutilus rutilus*	N	N	N	N	Y	N	N	N	Ranåker et al. (2012)
yellow perch *Perca flavescens*	cladoceran *Daphnia pulicaria*	N	N	Y	N	Y	N	Y	N	Richmond et al. (2004)
Miry's demoiselle *Neopomacentrus miryae*	brine shrimp *Artemia salina*	N	N	Y	N	Y	N	N	N	Rickel and Genin (2005)
Arctic grayling *Thymallus arcticus*	cladoceran *Bosmina longirostris*	N	N	N	N	Y	N	N	N	Schmidt and O'Brien (1982)
Arctic grayling *Thymallus arcticus*	copepod *Cyclops scutifer*	N	N	N	N	Y	N	N	N	Schmidt and O'Brien (1982)
Arctic grayling *Thymallus arcticus*	cladoceran *Daphnia longiremis*	N	N	N	N	Y	N	N	N	Schmidt and O'Brien (1982)
Arctic grayling *Thymallus arcticus*	cladoceran *Daphnia pulex*	N	N	N	N	Y	N	N	N	Schmidt and O'Brien (1982)
Arctic grayling *Thymallus arcticus*	copepod *Heterocope septentrionalis*	N	N	N	N	Y	N	N	N	Schmidt and O'Brien (1982)

Predator	Prey	Criteria								Source
		1	2	3	4	5	6	7	8	
flavescent peacock *Aulonocara stuartgranti*	brine shrimp *Artemia* sp. (dead)	N	N	Y	N	Y	N	N	N	Schwalbe et al. (2015)
flavescent peacock *Aulonocara stuartgranti*	brine shrimp *Artemia* sp. (living)	N	N	Y	N	Y	N	N	N	Schwalbe et al. (2015)
Tramitichromis sp.	brine shrimp *Artemia* sp. (dead)	N	N	Y	N	Y	N	N	N	Schwalbe et al. (2015)
Tramitichromis sp.	brine shrimp *Artemia* sp. (living)	N	N	Y	N	Y	N	N	N	Schwalbe et al. (2015)
brook trout *Salvelinus fontinalis*	housefly *Musca domestica*	N	N	Y	N	Y	N	N	N	Sweka and Hartman (2001)
smallmouth bass *Micropterus dolomieu*	housefly *Musca domestica*	N	N	Y	N	Y	N	N	N	Sweka and Hartman (2003)
two-spotted goby *Gobius flavescens*	**copepod (red mobile) *Calanus finmarchicus* *C. helgolandicus***	**N**	**Y**	**Y**	**C**	**Y**	**N**	**N**	**N**	**Utne-Palm (1999)**
two-spotted goby *Gobius flavescens*	**copepod (transparent immobile) *Calanus finmarchicus* *C. helgolandicus***	**N**	**Y**	**Y**	**C**	**Y**	**N**	**N**	**N**	**Utne-Palm (1999)**
two-spotted goby *Gobius flavescens*	**copepod (transparent mobile) *Calanus finmarchicus* *C. helgolandicus***	**N**	**Y**	**Y**	**C**	**Y**	**N**	**N**	**N**	**Utne-Palm (1999)**
two-spotted goby *Gobius flavescens*	copepod (10 prey) *Acartia clausi*	N	Y	Y	N	Y	N	N	N	Utne (1997)

Predator	Prey	Criteria								Source
		1	2	3	4	5	6	7	8	
two-spotted goby *Gobius flavescens*	copepod (1 prey) *Calanus finmarchicus*	Y	Y	Y	N	Y	N	N	N	Utne (1997)
two-spotted goby *Gobius flavescens*	**copepod (10 prey) *Calanus finmarchicus***	**Y**	**Y**	**Y**	**Y**	**Y**	N	**N**	**N**	**Utne (1997)**
bluegill *Lepomis macrochirus*	cladoceran *Daphnia pulex*	Y	N	Y	Y	Y	N	N	N	Vinyard and O'Brien (1976)
lake trout *Salvelinus namaycush*	cutthroat trout *Oncorhynchus clarkii clarkii*	Y	Y	Y	Y	Y	N	U	N	Vogel and Beauchamp (1999)
lake trout *Salvelinus namaycush*	rainbow trout *Oncorhynchus mykiss*	Y	Y	Y	Y	Y	N	U	N	Vogel and Beauchamp (1999)

Case #1: Chinook salmon reacting to rainbow trout

Hansen et al. (2013) conducted experiments where piscivorous yearling Chinook salmon *Oncorhynchus tshawytscha* reacted to live juvenile rainbow trout *O. mykiss* under varying levels of light and turbidity. One or two predators were used for each experimental trial. Prey fish were tethered inside clear acrylic tubes during experiments to minimize the potential for non-visual stimuli. However, as light levels decreased, the distance where Chinook salmon reacted to prey approached an asymptote at approximately 50 cm, potentially owing to a response to a non-visual stimulus that may have been an artifact of experimental design.

Lighting for the experiments was generated by lamps with a spectral output of 380–760 nm, placed 2.4 m above the water surface within the experimental arena. Light intensity was manipulated using dimmer switches and fiberglass window screens placed between the lamp and a diffuser plate. Light was measured in lux using an LI-COR LI-210 cosine corrected photometric sensor with a spectral sensitivity from 380–770 nm and in quantum flux using an LI-190 cosine corrected terrestrial quantum sensor with a spectral sensitivity from 400–700 nm. Turbidity was generated by mixing pulverized kaolin into the experimental arena using a pump. For experimental trials, the authors measured turbidity in nephelometric turbidity units (NTU) using a LaMotte Model 2020e nephelometer. The authors reported a conversion between NTU and beam attenuation coefficient, c ($c = 0.40 \times \text{NTU}$), at a wavelength of 660 nm based on transmittance measurements obtained using a Milton Roy Spectronic 21 DV spectrophotometer with a 10 mm path length cuvette. Because measurements were not corrected for forward scattering, conversion between NTU and c reported by Hansen et al. (2013) was more likely to approximate the effective attenuation coefficient, κ. We fit models to the original data from Hansen et al. (2013).

Case #2: Two-spotted goby reacting to ten copepods

Utne (1997) conducted microcosm experiments where two-spotted goby *Gobius flavescens* reacted to *Calanus finmarchicus*, a transparent calanoid copepod, under varying levels of light and turbidity. Prey were added to the experimental tanks in clear glass vials, each containing 10 copepods. Lighting for the experiments was provided using three halogen lamps, directed at the white walls of the experimental room. Diffuse light conditions were maintained in the experimental tanks by placing tanks in a white linen tent. Light intensity was manipulated by shielding the halogen lamps with perforated metal sheets. Light was measured using a Biospherical Instruments QSP-170B with a QSR-240 quantum scalar reference sensor which, per the manufacturer, has a spectral response within ±10% of 400-700 nm. Turbidity was generated by mixing diatomaceous earth into experimental arenas, and maintained using a perforated bubbling tube. To characterize turbidity, Utne (1997) measured absorbance at 800 nm using a Shimadzu UV-VIS Recording Spectrophotometer UV-160 with a 100 mm path length cuvette.

For Case #2, we digitized reaction distances from individual reactions from Utne (1997). Utne (1997) measured absorbance in units of cm^{-1}, but axis titles in the paper were erroneously labeled in units of m^{-1} (A.C. Utne-Palm, personal communication, May 21, 2019). Thus, we

multiplied absorbances by 100, and treated absorbance values as the effective attenuation coefficient, κ, for model fitting.

Case #3: Two-spotted goby reacting to single copepods

Utne-Palm (1999) measured the reaction of two-spotted goby to single *Calanus finmarchicus/Calanus helgolandicus* prey under varying levels of turbidity and a light intensity of 20 μE m^{-2} s^{-1}. Copepod treatments included mobile transparent, immobile transparent (glued to a glass coverslip), and mobile red-colored prey. As in Case #2, prey were inside glass vials for experiments. Light and turbidity were manipulated and measured using the same methods as Case #2. For Case #3, we digitized mean reaction distance data from Utne-Palm (1999).

Case #4: Stone moroko reacting to Daphnia pulex

Asaeda et al. (2002) measured the reaction distance and nadir viewing angle of stone moroko *Pseudorasbora parva* predators reacting to 0.8-1.0 mm *Daphnia pulex* prey under varying levels of light and turbidity. Free-swimming live prey were introduced to the experimental tanks containing a single predator, and data were collected until 20 reactions were recorded. Lighting was generated using fluorescent lamps that were partly covered by black paper and positioned 70 cm above the tanks. Turbidity was generated using kaolin. The authors did not report what equipment was used to obtain measurements of light and turbidity.

For Case #4, we digitized reaction distances from individual reactions from Asaeda et al. (2002). Measurement units reported in the study were incompatible with our models, so we transformed the data. The authors reported reaction distance in terms of predator body lengths. Predators used in the experiments were 50-60 mm, so we converted reaction distances to meters assuming a predator body length of 55 mm. Sagittal viewing angles were reported relative to a horizontal plane, where "upward" angles were positive and "downward" angles were negative, so we converted sagittal viewing angles to nadir viewing angles. Turbidity was reported as NTU, but no conversion to beam attenuation was provided and, for clear-water treatments, turbidity measurements were reported as NTU < 1. No measurements of the vertical attenuation coefficient were reported. For clear-water treatments, we assumed turbidity was the same as clear-water treatments in Case #1 (0.352 NTU), and converted NTU to the effective attenuation coefficient, κ, using the NTU to absorbance conversion for kaolin from Hansen et al. (2013). There is no direct relationship between the beam attenuation coefficient, c, and the diffuse attenuation coefficient, k_d, or between the effective attenuation coefficient, κ, and k_d. The true relationship between the beam attenuation coefficient and diffuse attenuation coefficient varies depending on factors such as the scattering phase function and radiance structure of the light field (Baker and Smith, 1979; Gordon, 1989). In natural marine waters, the beam attenuation coefficient, c, in the visible spectrum is often 2–4 times the vertical attenuation coefficient (Duntley, 1967). We conducted a preliminary sensitivity analysis and determined that model performance was relatively insensitive to conversions ranging from $k_d = c$ through $k_d = c/5$, so we assumed $k_d = c/3$, the middle of Duntley's range. Although Asaeda et al. (2002) reported light intensity in lux, we did not transform light intensity data to quantum units prior to model fitting because the authors did not report a conversion. However, we note that post-hoc transformation could be applied to scale T and convert K_e to units of μmol·photons·$m^{-2}$$s^{-1}$.

Model fitting

Variance increased as reaction distance increased in each case, so we assumed reaction distances had log-normally distributed error. We estimated separate variances for visual, σ_V, and non-visual, σ_{NV}, components of models because they involve different predator sensory processes that would presumably have different residual error structures.

We fit models to data using constrained maximum likelihood estimation with the quasi-Newton L-BFGS-B algorithm. We imposed parameter constraints to ensure the parameter space was restricted to physically and biologically plausible values. We fit models and estimated 95% confidence intervals for parameters using R package 'bbmle' (Bolker, 2017).

For computational efficiency, we used the Lambert W function (i.e. product logarithm function), $W(\cdot)$, to numerically approximate r_V in the Aksnes and Utne model and generalized visual reaction distance model. As an example, for the generalized visual reaction distance model:

$$r_V = W\left(0.5 \times (\kappa - k_d \cos\theta) \times \left(\omega(\kappa)|C_0|A_p E' \frac{E_b}{K_e + E_b}\right)^{0.5}\right) \times \left(\frac{2}{\kappa - k_d \cos\theta}\right). \qquad (B1)$$

Data and R code

Data and R code for cases are available via an online GitHub repository (Sean-Rohan-NOAA/GVRDM). A gold-standard back-up of the data and code are maintained by NOAA's Alaska Fisheries Science Center.

Appendix C: Empirical visual encounter distance model

For Case #1, we sought to compare the fit of an empirical visual encounter distance model to the Aksnes and Utne model and generalized visual reaction distance model. To do so, we used a continuous version of Hansen et al.'s (2013) broken-stick model (BSM). We chose the broken stick model because it was the most parsimonious empirical model out of four considered by Hansen et al. (2013). Hansen et al. (2013) parameterized the broken stick model by fitting separate models between turbidity and reaction distance (at a light intensity of ~50 lx), and light and reaction distance (at turbidity of 0.352 NTU):

$$r = \begin{cases} v + w\mathrm{E}_b & if\ E_b \le q_E \\ r_{maxE} & if\ E_b > q_E \end{cases}, \quad (C1)$$

$$r = \begin{cases} r_{maxc} & if\ c \le q_c \\ ue^{yc} & if\ c > q_c \end{cases}, \quad (C2)$$

where Eqn. B1 is the equation for light and Eqn. B2 is the equation for turbidity (see Table 3 for description of terms). Model parameters from Eqn. B1 and Eqn. B2 were subsequently used in a continuous model by Hansen et al. (2013) and Hansen and Beauchamp (2015), obtained by setting $u = e^{-\mathrm{y}q_c}$:

$$r = \begin{cases} (v + wE_b)p & if \quad E_b > q_E \\ pr_{max}p & if \quad E_b > q_E \end{cases}, \quad (C3)$$

$$p = \begin{cases} 1 & if \quad c \le q_c \\ ue^{yc} & if \quad c > q_c \end{cases}. \quad (C4)$$

For this study, we rearranged Eqn. B3 and B4 to create an equivalent form of the broken stick model, as:

$$r = \begin{cases} (v + wE_b)p & if\ E_b > q_E \\ r_{max}p & if\ E_b \le q_E \end{cases} \quad (C5)$$

$$p = \begin{cases} 1 & if\ c \le q_c \\ e^{y(c-q_c)} & if\ c > q_c \end{cases}. \quad (C6)$$

Appendix D: Residual plots

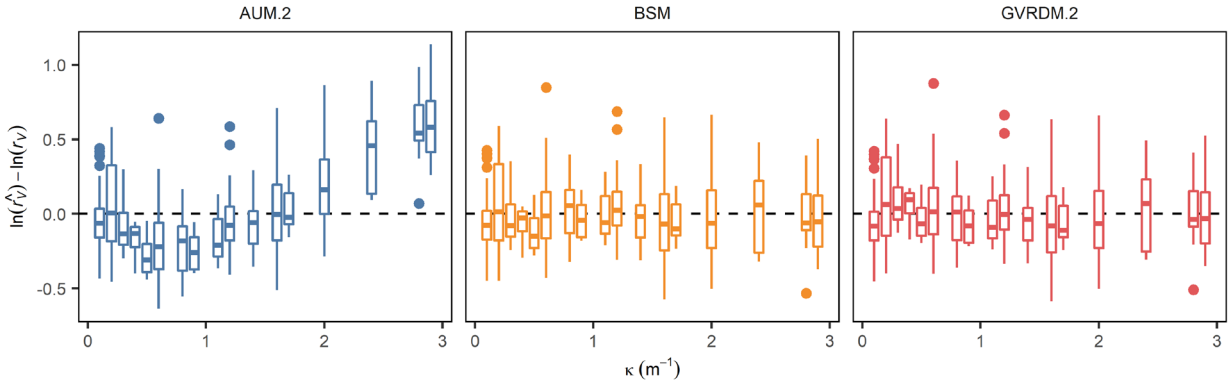

Figure D1. Case #1—Boxplot of visual reaction distance residuals from the Aksnes and Utne model with a non-visual reaction (AUM.2), the generalized visual reaction distance model with a non-visual reaction, without β (GVRDM.2), and the empirical broken-stick model (BSM) along a gradient of effective attenuation coefficient, κ, grouped by treatment level.

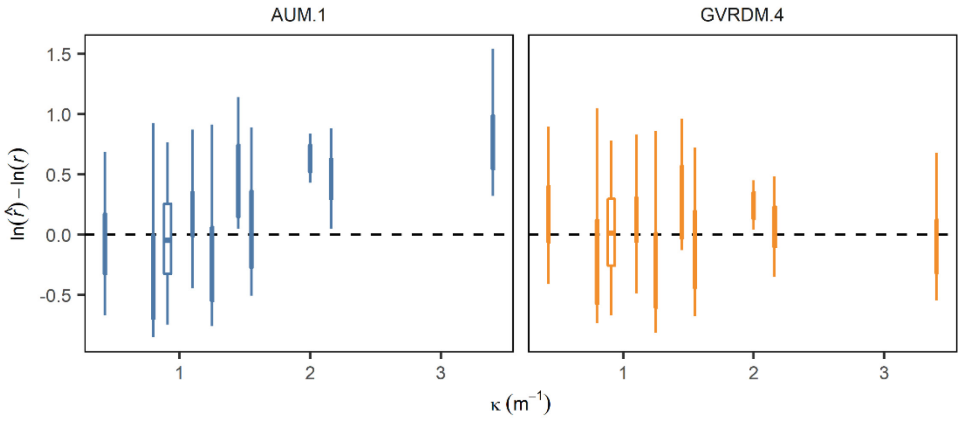

Figure D2. Case #2— Boxplot of reaction distance residuals from the Aksnes and Utne model (AUM.1) and generalized visual reaction distance model without a non-visual reaction or β (GVRDM.4) along a gradient of effective attenuation coefficient, κ, grouped by treatment level.

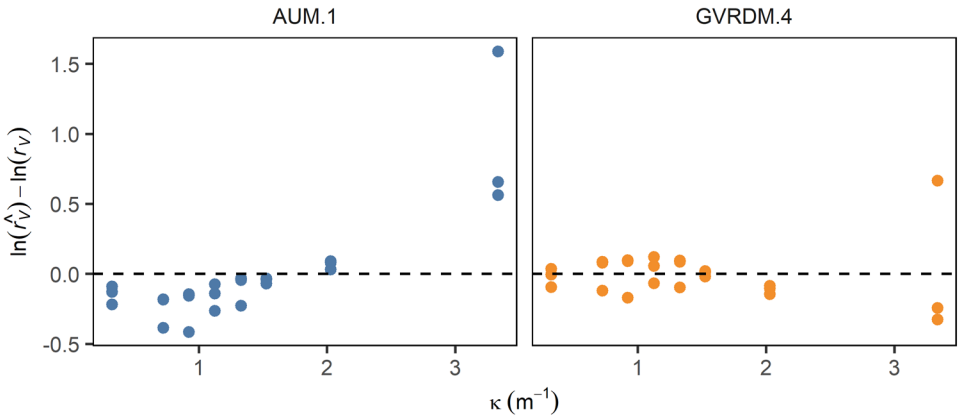

Figure D3. Case #3—Boxplot of reaction distance residuals from the Aksnes and Utne model (AUM.1) and generalized visual reaction distance model without a non-visual reaction or β (GVRDM.4) along a gradient of effective attenuation coefficient, κ, grouped by κ treatment level.

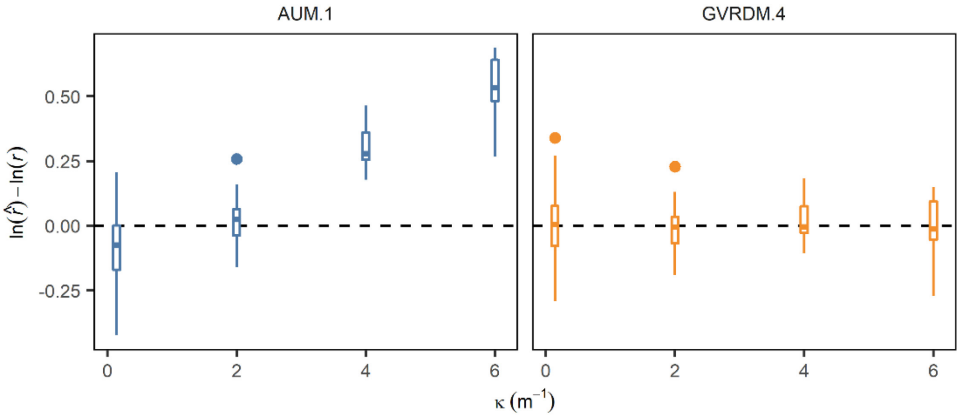

Figure D4. Case #4—Boxplot of visual reaction distance residuals of the Aksnes and Utne model (AUM.1) and generalized visual reaction distance model without a non-visual reaction or β (GVRDM.4) along a gradient of effective attenuation coefficient, κ, grouped by κ treatment level.

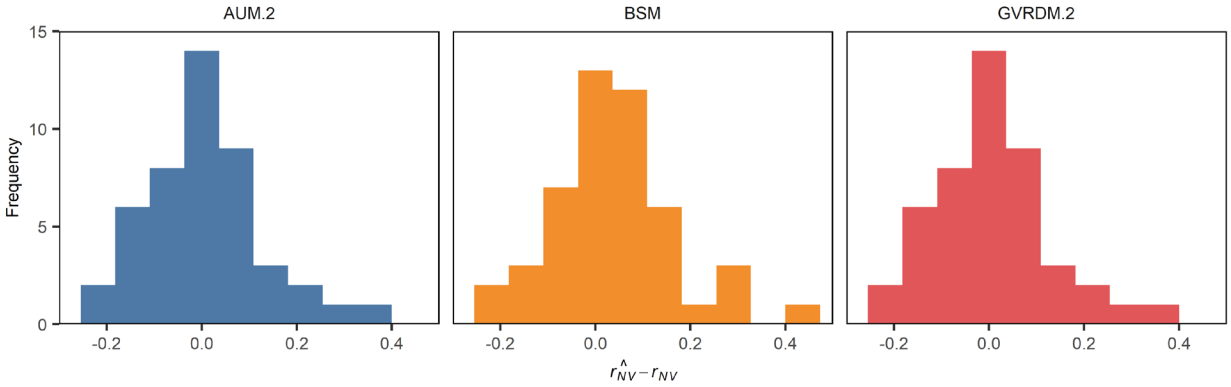

Figure D5. Case #1—Histogram of non-visual reaction distance residuals for the Aksnes and Utne model with a non-visual reaction (AUM.2), the generalized visual reaction distance model with-non visual reaction, without β (GVRDM.2), and the empirical broken-stick model (BSM). Non-visual reaction distances are for the subset of reactions estimated as non-visual reactions (i.e., $E_b < q$) in AUM.2 and GVRDM.2.

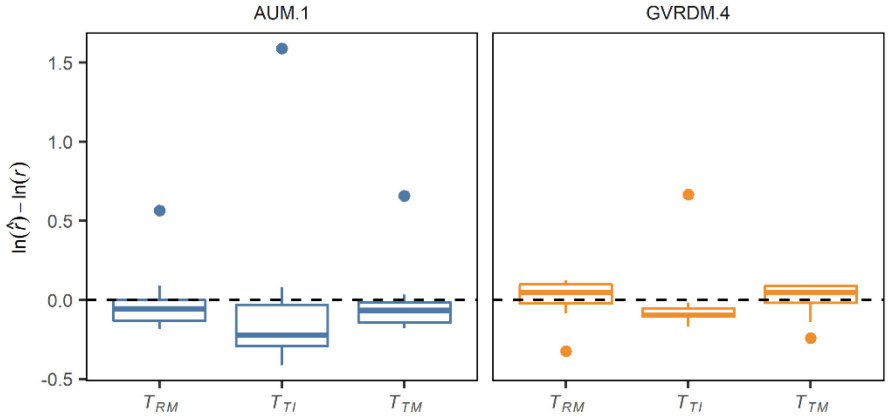

Figure D6. Case #3—Boxplots of error residuals of the Aksnes and Utne model (AUM.1) and the generalized visual reaction distance model without a non-visual reaction or β (GVRDM.4) for different copepod prey types. On the horizontal axis, *Calanus finmarchicus/helgolandicus* prey are denoted as: RM—red mobile, TI—transparent immobile, and TM—transparent mobile.

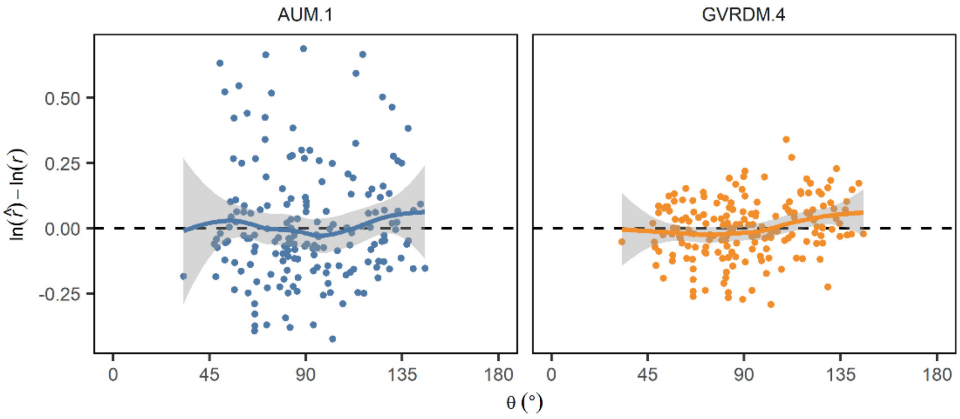

Figure D7. Case #4—Residuals of the Aksnes and Utne model (AUM.1) and the generalized visual reaction distance model without a non-visual reaction or β (GVRDM.4) along a gradient of sagittal viewing angle, θ. Lines and shaded areas denote the fit (mean ±2 standard errors) of loess models to residuals.

Appendix E: Pseudoreplication, attenuation coefficients, and angular dependence

Pseudoreplication

Aside from Case #3, we fit models to multiple reaction distances from single experimental trials, without accounting for pseudoreplication. To evaluate whether pseudoreplication affected the outcomes of model comparisons, we fit models to mean reaction distances for individual trials from Case #1. Aggregating reaction distance data by treatment level did not affect model ranking (Table E1).

Table E1. Model fits to mean reaction distances for Case #1, accounting for pseudoreplication.

Model	Par. (#)	n	ΔAIC_c
AUM.2	6	83	73.0
GVRDM.1	9	83	1.7
GVRDM.2	**8**	**83**	**0.0**
BSM	7	83	10.2

Attenuation coefficients

Absorbances derived from spectrophotometer or beam transmissometer measurements do not necessarily approximate the beam attenuation coefficient, *c*. Forward scattered light can cause light that has been scattered out of a collimated beam to reach the detector of a spectrophotometer or beam transmissometer, causing a positive bias in measured transmittance, leading to an underestimation of the beam attenuation coefficient (Zaneveld et al., 1979). Measurement biases are typically higher when path lengths are short, detector acceptance angles are wide (>1°), media are highly scattering, and transmitted wavelengths are prone to forward scattering (Kirk, 2011).

Because the Aksnes and Utne model is based on the law of contrast reduction, Aksnes and Utne (1997) corrected for forward scattering and spectrophotometer acceptance angle based on Jackson Turbidity Units, spectrophotometer absorbance, spectrophotometer path length, and the half-angle acceptance of the detector of the spectrophotometer, prior to model fitting.

Although we assumed the law of contrast reduction is violated in aquatic predator-prey interactions for our primary analyses, we sought to determine whether adjusting the absorbances to estimate the beam attenuation coefficient, rather than using raw absorbances, would affect our conclusions. Therefore, using data from Case #2, we followed the approach of Aksnes and Utne (1997), to calculate beam attenuation coefficients. We then fit models using the beam attenuation coefficient, *c*, instead of the effective attenuation coefficient, κ. Using beam attenuation, the generalized visual reaction distance model had a better fit to Case #2 data than the Aksnes and Utne model, based on lower AIC_c values (Table E2).

Table E2. Summary of model fits to Case #2 data with corrected beam attenuation coefficient, *c*.

Model	Par. (#)	n	ΔAICc
Case #2			
AUM.1	3	214	13.94
GVRDM.3	6	214	0.21
GVRDM.4	**5**	**214**	**0.0**

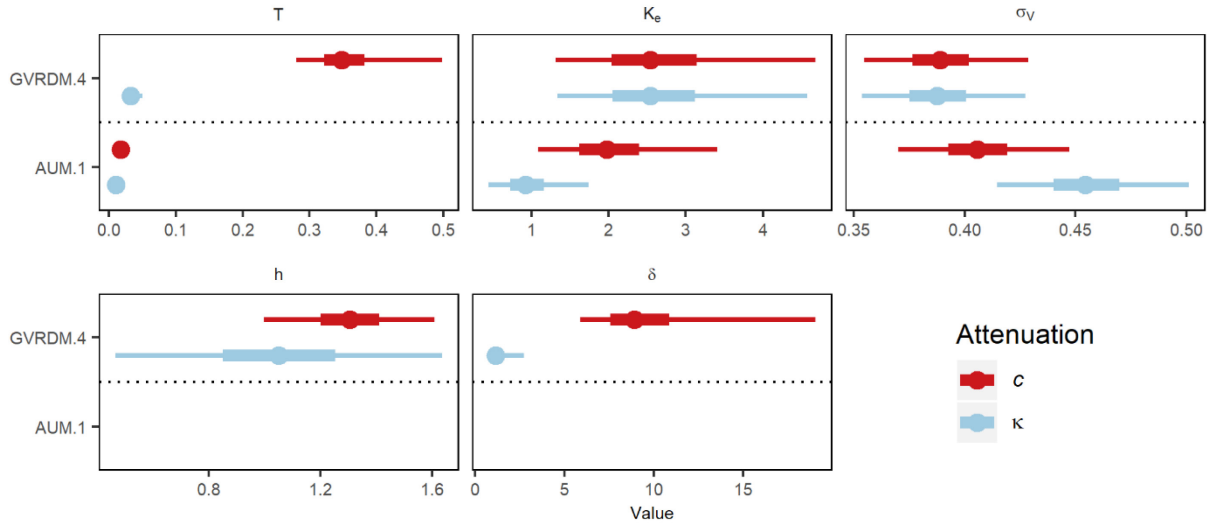

Figure E2. Parameter estimates for Case #2 data where spectrophotometer absorbance measurements were used as a proxy for the effective attenuation coefficient, κ, and where the beam attenuation coefficient, c, was estimated by adjusting absorbance measurements. Parameter estimates are shown for the generalized visual reaction distance model without a non-visual reaction or β (GVRDM.4) and the Aksnes and Utne model (AUM.1). Circles denote the means, thick lines denote 50% confidence intervals, thin lines denote 95% confidence intervals.

Angular dependence

Using data from Case #4, we evaluated whether accounting for nadir viewing angle, θ, in visual predator-prey interactions improved the fit of the generalized visual reaction distance model to data. To do so, we compared versions of the model where viewing angle data were included in the model to versions where viewing angle equaled 90°. The latter approach has typically been used to fit visual encounter distance models to experimental data. We found that including nadir viewing angle improved model fit, based on AIC_c (Table F3).

Table E3. Fits of the generalized visual reaction distance model to mean reaction distances from Case #4 assuming $\theta = 90°$ versus using observed values of θ.

Model	Par. (#)	n	AIC_c	ΔAIC_c
Assume $\theta = 90°$				
GVRDM.3	6	177	-254.0	2.8
GVRDM.4	5	177	-254.9	1.9
Observed θ				
GVRDM.3	6	177	-255.8	1.0
GVRDM.4	5	177	-256.8	0.0

Appendix F: Asymptotic equivalence between empirical and mechanistic models

Several studies have used Michaelis-Menten (e.g. Holling type-II) functions to model the relationship between light intensity and visual reaction distance under constant, clear-water conditions (i.e. low beam attenuation, low effective attenuation coefficient). Michaelis-Menten functions are structurally equivalent to a Naka-Rushton function with α=1. Here, we demonstrate that at low levels of turbidity and over short reaction distances, Michaelis-Menten models are an asymptotic approximation of the Aksnes and Utne model and generalized visual reaction distance model. Equations below are show using the symbols used by study authors and units of measure are shown using bracket notation (e.g. [m]).

Examples of Michaelis-Menten models are Richmond et al.'s (2004) model of age-0 yellow perch *Perca flavescens* reacting to *Daphnia pulicaria*, Holbrook et al.'s (2013) model of age-0 lake trout *Salvelinus namaycush* reacting to *Daphnia magna*, Keyler et al.'s (2015) model of siscowet lake trout *Salvelinus namaycush siscowet* reacting to golden shiner *Notemigonus crysoleucas*, and Keyler et al.'s (2019) model of siscowet lake trout *Salvelinus namaycush siscowet* reacting to deepwater sculpin *Myoxocephalus thompsonii*. In their models:

$$R_d[\mathrm{cm}] = \frac{R_{\max}[\mathrm{cm}] \cdot L_i[\mathrm{lux}]}{\alpha[\mathrm{lux}] + L_i[\mathrm{lux}]}, \tag{F1a}$$

or

$$R_d[\mathrm{cm}] = \frac{R_{\max}[\mathrm{cm}] \cdot L_i[\mathrm{photons} \cdot \mathrm{m}^{-2} \cdot \mathrm{s}^{-1}]}{\alpha[\mathrm{photons} \cdot \mathrm{m}^{-2} \cdot \mathrm{s}^{-1}] + L_i[\mathrm{photons} \cdot \mathrm{m}^{-2} \cdot \mathrm{s}^{-1}]}, \tag{F1b}$$

where R_d is reaction distance, R_{max} is maximum reaction distance, L_i is light intensity, and α is a half-saturation constant. Similarly, Hansen et al. (2013) considered a Holling type-II function with an intercept as a candidate for modeling the reaction distance of yearling Chinook salmon to juvenile rainbow trout (i.e. Case #1):

$$RD[\mathrm{cm}] = C[\mathrm{cm}] + \frac{A[\mathrm{cm}]I[\mathrm{lux}]}{B[\mathrm{lux}] + I[\mathrm{lux}]} \tag{F2}$$

where RD is reaction distance, C is the reaction distance asymptote at low light, A is a parameter which represents the maximum visual reaction distance that is added to C, B is a half-saturation constant, and I is light intensity.

In the Aksnes and Utne model, as beam attenuation, c, and viewing distance, r_V, approach 0, e^{cr_V} approaches 1. Setting $e^{cr_V} = 1$ results in:

$$r_V^2[\mathrm{m}^2] = \frac{T[\mathrm{m}^2] \cdot E_b[\mu\mathrm{E} \cdot \mathrm{m}^2 \cdot \mathrm{s}^{-1}]}{K_e[\mu\mathrm{E} \cdot \mathrm{m}^2 \cdot \mathrm{s}^{-1}] + E_b[\mu\mathrm{E} \cdot \mathrm{m}^2 \cdot \mathrm{s}^{-1}]}. \tag{F3}$$

Similarly, in the generalized visual reaction distance model, as the effective attenuation coefficient, κ, and r_V approach 0, $e^{\kappa r_V}$ approaches 1. For the generalized visual reaction distance model, setting $e^{\kappa r_V} = 1$ results in:

$$r_V^2[\mathrm{m}^2] = \omega(\kappa) \frac{T[\mathrm{m}^2] \cdot E_b[\mu\mathrm{E} \cdot \mathrm{m}^2 \cdot \mathrm{s}^{-1}]}{K_e[\mu\mathrm{E} \cdot \mathrm{m}^2 \cdot \mathrm{s}^{-1}] + E_b[\mu\mathrm{E} \cdot \mathrm{m}^2 \cdot \mathrm{s}^{-1}]}, \tag{F4}$$

where $\omega(\kappa)$ is a constant.

Most visual encounter distance experiments measure light using the same general approach, regardless of differences in measurement units. Therefore, light quantities in equations F1–F4 are interchangeable if: $E_b \propto L_i \propto I$. Quantities R_{max} and T can be converted using $R_{max}/100[m] = \sqrt{T}[m]$, while r_V^2 and R_d can be converted using $R_d/100[m] = \sqrt{r_V^2}[m]$. Thus, through unit conversion:

$$\frac{E_b\sqrt{T}}{K_e + E_b} = \frac{L_i\left(\frac{R_{max}}{100}\right)}{\alpha + L_i} = \frac{I\left(\frac{A}{100}\right)}{B + I} + 0. \qquad (F5)$$

This shows that the models are effectively equal under clear-water conditions and over short distances.

Disclaimer

Any use of trade, firm, or product names is for descriptive purposes only and does not imply endorsement by the U.S. Government.

References

Aksnes, D.L., Utne, A.C.W., 1997. A revised model of visual range in fish. Sarsia 82, 137–147. https://doi.org/10.1080/00364827.1997.10413647

Asaeda, T., Park, B.K., Manatunge, J., 2002. Characteristics of reaction field and the reactive distance of a planktivore, *Pseudorasbora parva* (Cyprinidae), in various environmental conditions. Hydrobiologia 489, 29–43. https://doi.org/10.1023/A:1023298823106

Baker, K.S., Smith, R.C., 1979. Quasi-inherent characteristics of the diffuse attenuation coefficient for irradiance. Ocean Opt. IV 208, 60–63.

Barrett, J.C., Grossman, G.D., Rosenfeld, J., 1992. Turbidity-induced changes in reactive distance of rainbow trout. Trans. Am. Fish. Soc. 121, 437–443. https://doi.org/10.1577/1548-8659(1992)121<0437:TICIRD>2.3.CO;2

Bolker, B.M., 2017. bbmle: Tools for General Maximum Likelihood Estimation.

Breck, J.E., Gitter, M.J., 1983. Effect of fish size on the reactive distance of bluegill (*Lepomis macrochirus*) sunfish. Can. J. Fish. Aquat. Sci. 40, 162–167. https://doi.org/10.1139/f83-026

Chesney, E.J., 2008. Foraging behavior of bay anchovy larvae, Anchoa mitchilli. J. Exp. Mar. Bio. Ecol. 362, 117–124. https://doi.org/10.1016/j.jembe.2008.06.011

Confer, J.L., Howick, G.L., Corzette, M.H., Kramer, S.L., Fitzgibbon, S., Landesberg, R., 1978. Visual predation by planktivores. Oikos 31, 27–37.

Crowl, T.A., 1989. Effects of crayfish size, orientation, and movement on the reactive distance of largemouth bass foraging in clear and turbid water. Hydrobiologia 183, 133–140.

Djamgoz, M.B.A., Yamada, M., 1990. Electrophysiological characteristics of retinal neurones: synaptic interactions and functional outputs, in: Douglas, R., Djamgoz, M. (Eds.), The Visual System of Fish. Chapman and Hall, New York, NY, pp. 159–210.

Duntley, S.Q., 1967. Visibility in the oceans. Opt. Spectra Fourth Qua, 64–69. https://doi.org/10.1166/jnn.20

Duntley, S.Q., 1952. The visibility of submerged objects. Cambridge, Massachusetts.

Duntley, S.Q., 1948. The reduction of apparent contrast by the atmosphere. J. Opt. Soc. Am. 38, 179–191.

Gordon, H.R., 1989. Can the Lambert-Beer law be applied to the diffuse attenuation coefficient of ocean water? Limnol. Oceanogr. 34, 1389–1409. https://doi.org/10.1097/00003246-200206000-00018

Gregory, R.S., Northcote, T.G., 1993. Surface, planktonic, and benthic foraging by juvenile Chinook salmon (*Oncorhynchus tshawytscha*) in turbid laboratory conditions. Can. J. Fish. Aquat. Sci. 50, 233–240.

Hansen, A.G., Beauchamp, D.A., Schoen, E.R., 2013. Visual prey detection responses of piscivorous trout and salmon: Effects of light, turbidity, and prey size. Trans. Am. Fish. Soc. 142, 854–867. https://doi.org/10.1080/00028487.2013.785978

Hecht, T., van der Lingen, C.D., 1992. Turbidity-induced changes in feeding strategies of fish in estuaries. South African J. Zool. 27, 95–107. https://doi.org/10.1080/02541858.1992.11448269

Henderson, M.A., Northcote, T.G., 1985. Visual prey detection and foraging in sympatric cutthroat trout (Salmo clarki clarki) and Dolly Varden (Salvelinus malma). Can. J. Fish. Aquat. Sci. 42, 785–790.

Holbrook, B. V., Hrabik, T.R., Branstrator, D.K., Mensinger, A.F., 2013. Foraging mechanisms of age-0 lake trout (*Salvelinus namaycush*). J. Great Lakes Res. 39, 128–137. https://doi.org/10.1016/j.jglr.2012.12.008

Howick, G.L., O'Brien, W.J., 1983. Piscivorous feeding behavior of largemouth bass: an experimental analysis. Trans. Am. Fish. Soc. 112, 508–516. https://doi.org/10.1577/1548-8659(1983)112<508

Jönsson, M., Ranåker, L., Anders Nilsson, P., Brönmark, C., 2012. Prey-type-dependent foraging of young-of-the-year fish in turbid and humic environments. Ecol. Freshw. Fish 21, 461–468. https://doi.org/10.1111/j.1600-0633.2012.00565.x

Kaneko, A., 1971. Electrical connexions between horizontal cells in the dogfish retina. J. Physiol. 213, 95–105. https://doi.org/10.1113/jphysiol.1971.sp009370

Keyler, T.D., Hrabik, T.R., Austin, C.L., Gorman, O.T., Mensinger, A.F., 2015. Foraging mechanisms of siscowet lake trout (*Salvelinus namaycush siscowet*) on pelagic prey. J. Great Lakes Res. 41, 1162–1171. https://doi.org/10.1016/j.jglr.2015.09.016

Keyler, T.D., Hrabik, T.R., Mensinger, A.F., Rogers, L.S., Gorman, O.T., 2019. Effect of light intensity and substrate type on siscowet lake trout (*Salvelinus namaycush siscowet*) predation on deepwater sculpin (Myoxocephalus thompsonii). Hydrobiologia 840, 77–88. https://doi.org/10.1007/s10750-019-3944-5

Kirk, J.T.O., 2011. Light and photosynthesis in aquatic ecosystems, 3rd ed. Cambridge University Press, New York.

Langbehn, T.J., Varpe, Ø., 2017. Sea-ice loss boosts visual search: Fish foraging and changing pelagic interactions in polar oceans. Glob. Chang. Biol. 23, 5318–5330. https://doi.org/10.1111/gcb.13797

Lee, Z., Shang, S., Hu, C., Du, K., Weidemann, A., Hou, W., Lin, J., Lin, G., 2015. Secchi disk depth: A new theory and mechanistic model for underwater visibility. Remote Sens. Environ. 169, 139–149. https://doi.org/10.1016/j.rse.2015.08.002

Link, J., Edsall, T.A., 1996. The effect of light on lake herring (Coregonus artedi) reactive volume. Hydrobiologia 332, 131–140. https://doi.org/10.1007/BF00016692

Lythgoe, J.., 1972. The adaptation of visual pigments to the photic environment, in: Dartnell, H.J.A. (Ed.), The Handbook of Sensory Physiology VII/1. Springer, pp. 566–603.

Mazur, M.M., Beauchamp, D.A., 2003. A comparison of visual prey detection among species of piscivorous salmonids: Effects of light and low turbidities. Environ. Biol. Fishes 67, 397–405. https://doi.org/10.1023/A:1025807711512

Meager, J.J., Moberg, O., Strand, E., Utne-Palm, A., 2010. Effects of light intensity on visual prey detection by juvenile Atlantic cod (*Gadus morhua* L.). Mar. Freshw. Behav. Physiol. 43, 99–108. https://doi.org/http://dx.doi.org/10.1080/10236241003798910

Meager, J.J., Solbakken, T., Utne-Palm, A., Oen, T., 2005. Effects of turbidity on the reaction distance, search time, and foraging success of juvenile Atlantic cod (*Gadus morhua*). Can. J. Fish. Aquat. Sci. 62, 1978–1984. https://doi.org/10.1139/F05-104

Middleton, W.E.K., 1952. Vision through the atmosphere. University of Toronto Press.

Naka, K.I., Chan, R.Y., Yasui, S., 1979. Adaptation in catfish retina. J. Neurophysiol. 42, 441–454. https://doi.org/10.1152/jn.1979.42.2.441

Naka, K.I., Chappell, R.L., Sakuranaga, M., Ripps, H., 1988. Dynamics of skate horizontal cells. J. Gen. Physiol. 92, 811–831. https://doi.org/10.1085/jgp.92.6.811

Naka, K.I., Rushton, W.A.H., 1966a. S-potentials from luminosity units in the retina of fish (Cyprinidae). J. Physiol. 185, 587–599.

Naka, K.I., Rushton, W.A.H., 1966b. S-potentials from colour units in the retina of fish (Cyprinidae). J. Physiol. 185, 536–555.
Nieman, C.L., Gray, S.M., 2019. Visual performance impaired by elevated sedimentary and algal turbidity in walleye *Sander vitreus* and emerald shiner *Notropis atherinoides*. J. Fish Biol. 95, 186–199. https://doi.org/10.1111/jfb.13878
Preisendorfer, R.W., 1986. Secchi disk science: Visual optics of natural waters. Limnol. Oceanogr. 31, 909–926.
Quesenberry, N.J., Allen, P.J., Cech, J.J., 2007. The influence of turbidity on three-spined stickleback foraging. J. Fish Biol. 70, 965–972. https://doi.org/10.1111/j.1095-8649.2007.01350.x
Ranåker, L., Jönsson, M., Nilsson, P.A., Brönmark, C., 2012. Effects of brown and turbid water on piscivore-prey fish interactions along a visibility gradient. Freshw. Biol. 57, 1761–1768. https://doi.org/10.1111/j.1365-2427.2012.02836.x
Richmond, H.E., Hrabik, T.R., Mensinger, A.F., 2004. Light intensity, prey detection and foraging mechanisms of age 0 year yellow perch. J. Fish Biol. 65, 195–205. https://doi.org/10.1111/j.0022-1112.2004.00444.x
Rickel, S., Genin, A., 2005. Twilight transitions in coral reef fish: the input of light-induced changes in foraging behaviour. Anim. Behav. 70, 133–144. https://doi.org/10.1016/j.anbehav.2004.10.014
Ruxton, G.D., Johnsen, S., 2016. The effect of aggregation on visibility in open water. Proc. R. Soc. B Biol. Sci. 283.
Sakai, H.M., Wang, J.L., Naka, K.I., 1995. Contrast gain control in the lower vertebrate retinas. J. Gen. Physiol. 105, 815–835.
Schmidt, D., O'Brien, W.J., 1982. Planktivorous feeding ecology of Arctic grayling (*Thymallus arcticus*). Can. J. Fish. Aquat. Sci. 39, 475–482. https://doi.org/10.1155/2011/352451
Schwalbe, M.A.B., Webb, J.F., 2015. The effect of light intensity on prey detection behavior in two Lake Malawi cichlids, *Aulonocara stuartgranti* and *Tramitichromis* sp. J. Comp. Physiol. A Neuroethol. Sensory, Neural, Behav. Physiol. 201, 341–356. https://doi.org/10.1007/s00359-015-0982-y
Sweka, J.A., Hartman, K.J., 2003. Reduction of reactive distance and foraging success in smallmouth bass, *Micropterus dolomieu*, exposed to elevated turbidity levels. Environ. Biol. Fishes 67, 341–347. https://doi.org/10.1023/A:1025835031366
Sweka, J.A., Hartman, K.J., 2001. Influence of turbidity on brook trout reactive distance and foraging success. Trans. Am. Fish. Soc. 130, 138–146. https://doi.org/10.1577/1548-8659(2001)130<0138:iotobt>2.0.co;2
Utne-Palm, A., 1999. The effect of prey mobility, prey contrast, turbidity and spectral composition on the reaction distance of *Gobiusculus flavescens* to its planktonic prey. J. Fish Biol. 54, 1244–1258. https://doi.org/10.1111/j.1095-8649.1999.tb02052.x
Utne, A., 1997. The effect of turbidity and illumination on the reaction distance and search time of the marine planktivore *Gobiusculus flavescens*. J. Fish Biol. 50, 926–938. https://doi.org/10.1111/j.1095-8649.1997.tb01619.x
Vinyard, G.L., O'Brien, W.J., 1976. Effects of light and turbidity on the reactive distance of bluegill (*Lepomis macrochirus*). J. Fish. Res. Board Canada 33, 2845–2849.
Vogel, J.L., Beauchamp, D.A., 1999. Effects of light, prey size, and turbidity on reaction distances of lake trout (*Salvelinus namaycush*) to salmonid prey. Can. J. Fish. Aquat. Sci. 56, 1293–1297. https://doi.org/10.1139/cjfas-56-7-1293

Zaneveld, J.R., Spinrad, R.W., Bartz, R., 1979. Optical properties of turbidity standards. Ocean Opt. IV 208, 159–168.